

BRAKING THE GAS IN THE  $\beta$  PICTORIS DISKRODRIGO FERNÁNDEZ<sup>1</sup>, ALEXIS BRANDEKER, AND YANQIN WU

Department of Astronomy and Astrophysics, University of Toronto, 60 St. George Street, Toronto, ON M5S 3H8, Canada

Received 2005 September 8; Accepted 2005 December 28

## ABSTRACT

Metallic gas detected in the  $\beta$  Pictoris circumstellar debris disk raises many questions. The origin of this gas is unclear and its very presence is difficult to explain: many constituents of the gas are expected to be radiatively accelerated outward, yet their motion appears to be consistent with Keplerian rotation out to at least 300 AU. Hydrogen has previously been hypothesized to exist in the disk, acting as a braking agent, but the amount required to brake individual elements conflicted with observed upper limits.

To resolve this discrepancy, we search for alternative braking mechanisms for the metallic gas. We find that all species affected by radiation force are heavily ionized. Frequent Coulomb collisions couple the ions into a single fluid, reducing the radiation force on species feeling the strongest acceleration. For a gas of solar composition, the resulting total radiation force still exceeds gravity, while a gas of enhanced carbon abundance could be self-braking. We also explore two other braking agents: collisions with dust grains and neutral gas. Grains surrounding  $\beta$  Pic are photoelectrically charged to a positive electrostatic potential. If a significant fraction of the dust grains are carbonaceous (10% in the midplane and larger at higher altitudes), ions can be slowed down to satisfy the observed velocity constraints. In this case, both the gas kinematics and spatial distributions are expected to coincide with those of small grains, the latter being indeed observed. For neutral gas to brake the coupled ion fluid, we find the minimum required mass to be  $\approx 0.03 M_{\oplus}$ , consistent with observed upper limits of the hydrogen column density, and substantially reduced relative to previous estimates.

Our results favor a scenario in which metallic gas is generated by grain evaporation in the disk, perhaps during grain-grain collisions. We exclude a primordial origin for the gas, but cannot rule out the possibility of its production by falling evaporating bodies near the star. We discuss the implications of this work for observations of gas in other debris disks.

*Subject headings:* stars: individual ( $\beta$  Pictoris) — circumstellar matter — acceleration of particles — scattering — planetary systems: formation — planetary systems: protoplanetary disks

## 1. INTRODUCTION

The evolution of circumstellar disks is intimately connected to the process of star and planet formation. In the standard isolated low-mass star formation scenario (e.g., Shu, Adams & Lizano 1987), disks begin their existence as *protostellar* accretion disks, later turning into *protoplanetary* disks, once the newborn star reaches the T Tauri phase. The late evolutionary stages of circumstellar disks are not well understood. Once the star has reached the main sequence and the planet formation process is complete, the disk is thought to have been depleted of its primordial gas, keeping small amounts generated by either stellar winds or evaporation of solid bodies (e.g., Lagrange et al. 2000). In the few cases where late disks are observable, lifetimes of small dust grains ( $\lesssim 1 \mu\text{m}$ ) are shorter than the estimated ages of those systems, implying a dust replenishment mechanism (Backman & Paresce 1993). These kind of late circumstellar disks are usually referred to as *debris disks*. The gas lifetime in those systems, currently unknown, determines the maximum period over which protoplanetary cores can accrete gas and form gaseous planets (e.g., Bodenheimer & Lin 2002), and is related the formation of terrestrial planets and cores of giant planets by the increased efficiency of planetesimal accretion due to the presence of gas (Rafikov 2004).

So far, the best studied debris disk is that of  $\beta$  Pictoris, a nearby ( $19.3 \pm 0.2$  pc, Crifo et al. 1997), A5V star. The dust component of the disk has been extensively studied since it revealed itself as infrared excess in the stellar spectrum (Aumann et al. 1985). The favorable edge-on orientation has allowed direct imaging in thermal emission (Lagage & Pantin 1994), as well as in scattered light (Smith & Terrell 1984, Heap et al. 2000), indicating a disk size  $\sim 1000$  AU. The gas component has been more elusive. Freudling et al. (1995) set a  $3\sigma$  upper limit on the column density of H I,  $N_{\text{HI}} \leq 10^{19} \text{ g cm}^{-2}$ , by non-detection of the 21 cm line, while Thi et al. (2001) and Lecavelier des Etangs et al. (2001) searched for signatures of H<sub>2</sub> in the IR and UV, respectively, obtaining discrepant results:  $50 M_{\oplus}$  in the first case (corresponding to  $N_{\text{H}_2} \sim 3 \times 10^{21} \text{ cm}^{-2}$ ), and an upper limit  $N_{\text{H}_2} \leq 10^{18} \text{ cm}^{-2}$  ( $\sim 0.1 M_{\oplus}$ ) in the second. Metallic elements have been detected through stable and variable circumstellar lines (Hobbs et al. 1985; Ferlet et al. 1987). The variable, redshifted lines have been attributed to falling evaporating bodies (FEBs) in highly eccentric orbits (Ferlet et al. 1987), whereas the stable component has no well established explanation for its origin. Lagrange et al. (1998) proposed three possible gas formation scenarios: stellar wind, star-grazing comet evaporation, and dust grain evaporation near the star. Recent improvements in the gas characterization include spatially resolved emission lines from stable metallic species, which revealed them to be consistent with Keplerian rotation (Olofsson et al. 2001), and spatially extended out to at least 300 AU from the star (Brandeker et al. 2004).

It was realized early on (e.g., Beust et al. 1989) that certain elements in the gas disk of  $\beta$  Pic should be subject to a very strong

<sup>1</sup> e-mail: fernandez@astro.utoronto.ca

radiation force from the star, overcoming gravitational attraction. However, besides Keplerian rotation, stable lines do not show any substantial radial velocities relative to the star (e.g., Lagrange et al. 1998, Brandeker et al. 2004). This implies the presence of a braking mechanism acting in the disk.

The first model of how gas might be braked and produce the stable absorption lines was presented by Lagrange et al. (1998). They proposed a scenario in which gas is injected into the disk due to FEBs. Since neutral hydrogen is not affected by the stellar radiation force, it would accumulate in the region of gas generation, in the form of an annulus located a few AU from the star. The elements affected by radiation force would then be slowed down temporarily in this annular region, producing the observed stable absorption features. After passing this hydrogen-rich region, elements would then be accelerated again, leaving the system at high velocities. This model reproduces the stable absorption lines, and is consistent with the FEBs scenario for the variable lines. However, the fact that elements affected by radiation force reach high velocities after passage by the annulus, which extends only out to a few AU from the star, is incompatible with the emission from  $\sim 300$  AU. Brandeker et al. (2004) calculated the amount of material necessary to slow down the most strongly accelerated particles to within observational constraints by means of neutral-neutral collisions, finding that  $\sim 50 M_{\oplus}$  of hydrogen are needed. According to Thébault & Augereau (2005), there could be no more than  $0.4 M_{\oplus}$  of gas in the disk, as it would affect the dynamics of the dust to the degree that dust production models become incompatible with observations.

As an alternative braking mechanism, Brandeker (2004) explored the slowing down of ionized species by a large-scale magnetic field, concluding that only a toroidal field could remove the radial velocity components of ions. Brandeker (2004) showed that unless the field is stronger than  $\sim 1$  mG at 100 AU, this configuration would be unstable to currents generated by radiation force. He also raised the question of the origin of such an ad-hoc field geometry.

In this paper we address the braking of the stable metallic gas in the entire  $\beta$  Pic disk. Given the spectral type of the star and the fact that the disk is optically thin, we expect several gaseous species to be ionized. This prompts us to explore the role of Coulomb collisions among ionized gas particles, which may be an important braking agent due to the long range of electromagnetic interactions. We proceed then to explore the interaction of this ionized gas with dust grains, which are photoelectrically charged. Finally, we extend the study of Lagrange et al. (1998) to explore whether ion-neutral collisions are able to brake particles affected by radiation force far out in the disk, and the amount of neutral gas required to satisfy the observed velocity constraints.

The paper is organized as follows: in §2 we explore the physical conditions of the gas, and the constraints on the possible braking mechanisms that this imposes. In §3 we study ion-ion collisions, ion-grain collisions, and revisit ion-neutral interactions. In §4 we discuss the implications of our results for gas generation and extend it to similar systems. Our conclusions follow in §5.

## 2. SETTING THE STAGE FOR BRAKING

In this section we explore the physical environment of the gaseous disk. This will enable us to characterize the requirements the braking mechanisms have to satisfy.

### 2.1. Radiation Force

The radiation force  $F_{\text{rad}}$  acting on a given atom originates by a net momentum transfer due to scattering events,

$$F_{\text{rad}} = \frac{1}{c} \sum_{j < k} F_{\lambda} \sigma_{jk}, \quad (1)$$

where  $c$  is the speed of light,  $\sigma_{jk}$  is the cross section for the transition between atomic levels  $j$  and  $k$  integrated over wavelength, and  $F_{\lambda}$  is the stellar flux per unit wavelength evaluated at the line center. Since the stellar flux decays like the inverse square of the distance from the source, the ratio  $\beta$  between radiation and gravitational forces is distance-independent:

$$\beta \equiv \frac{F_{\text{rad}}}{F_{\text{grav}}} = \frac{1}{8\pi c^2} \frac{r^2}{GMm} \sum_{j < k} \frac{g_k}{g_j} A_{kj} \lambda_{jk}^4 F_{\lambda}, \quad (2)$$

where we have expressed  $\sigma_{jk}$  in terms of known atomic quantities (e.g., Hilborn 1982). Here,  $g_j$  and  $g_k$  are the statistical weights of levels  $j$  and  $k$ ,  $A_{kj}$  is the Einstein coefficient for spontaneous emission from level  $k$  to  $j$ ,  $\lambda_{jk}$  the wavelength of the corresponding transition,  $G$  is the gravitational constant,  $M$  the stellar mass, and  $m$  the mass of the atomic species under consideration.

The energy of a particle of mass  $m$  in a bound orbit with semi-major axis  $a$  around an object of mass  $M$  is  $E_{\text{bind}} = -GMm/(2a)$ . When the contribution of radiation is added, the energy of the system increases by an amount  $E_{\text{rad}} = \beta GMm/r$ , where  $r$  is the distance to the star at a given point in the orbit. For a circular orbit ( $r = a$ ), the particle ceases to be bound if  $\beta > 0.5$ . If  $\beta < 0.5$  the particle remains in a bound orbit, but “feeling” a lower dynamical mass  $(1 - \beta)M$ .

Values for  $\beta$  in this system are available in the literature for some elements, but we find it necessary to calculate a set of  $\beta$  values for as many elements as possible. The low temperatures and densities of the gas in the disk (at distances  $\gtrsim$  few AU from the star, see §2.2) imply that radiative de-excitations are faster than either collisions or radiative excitations, thus most atoms are in the ground state. This implies  $j = 0$  in equation (2), simplifying calculations considerably. Since we do not expect species to be more than twice ionized (see §2.2), we study the first three ionization states of elements from H to Ni. The atomic data are taken from the NIST Atomic Spectra Database version 2.0 (Martin et al. 1999)<sup>2</sup>. For elements with multiple ground states (e.g., Fe I), we assume that the population of each level is proportional to its statistical weight (e.g., Lagrange et al. 1996). The uncertainties in  $A_{k0}$  range from  $< 3\%$  for the strongest lines to  $\sim 100\%$  for the weakest.

The stellar flux is approximated with a PHOENIX model spectrum (Hauschildt, Allard & Baron 1999) for a star of effective temperature  $T_{\text{eff}} = 8000$  K and surface gravity  $\log g = 4.2$ . Given that  $\beta$  Pic is rotating at  $130 \pm 4$  km s<sup>-1</sup> (Royer et al. 2002), the

<sup>2</sup> <http://physics.nist.gov/asd2>

TABLE 1  
RADIATION FORCE COEFFICIENTS OBTAINED FROM ROTATIONALLY BROADENED  $\beta$  PIC-LIKE SPECTRUM

Ion	$\beta^{a,b}$	Ion	$\beta^b$	Ion	$\beta^{a,b}$	Ion	$\beta^{a,b}$
H I	$(1.6 \pm 0.1)10^{-3}$	F I	0	S I	$0.56 \pm 0.09$	V I	$72 \pm 4$
He I	0	F II	$(3.5 \pm 0.9)10^{-6}$	S II	$(9.0 \pm 1.0)10^{-5}$	V II	$4.4 \pm 0.2$
He II	...	F III	$(5.0 \pm 1.0)10^{-9}$	S III	$(2.0 \pm 1.0)10^{-4}$	V III	0
Li I	$900 \pm 40$	Ne I	0	Cl I	$(2.3 \pm 0.4)10^{-3}$	Cr I	$93 \pm 5$
Li II	0	Ne II	0	Cl II	$(3.7 \pm 0.4)10^{-7}$	Cr II	$(6.0 \pm 3.0)10^{-7}$
Li III	...	Ne III	$(9.0 \pm 2.0)10^{-8}$	Cl III	$(3.0 \pm 2.0)10^{-6}$	Cr III	...
Be I	$62 \pm 7$	Na I	$360 \pm 20$	Ar I	$(1.7 \pm 0.3)10^{-6}$	Mn I	$28 \pm 3$
Be II	$124 \pm 6$	Na II	0	Ar II	0	Mn II	$7 \pm 1$
Be III	0	Na III	0	Ar III	$(1.5 \pm 0.2)10^{-7}$	Mn III	...
B I	$30 \pm 10$	Mg I	$74 \pm 8$	K I	$200 \pm 20$	Fe I	$27 \pm 2$
B II	$0.07 \pm 0.04$	Mg II	$9 \pm 2$	K II	...	Fe II	$5.0 \pm 0.3$
B III	$19 \pm 1$	Mg III	0	K III	$(4.4 \pm 0.2)10^{-4}$	Fe III	$(3.0 \pm 0.6)10^{-7}$
C I	$(3.3 \pm 0.1)10^{-2}$	Al I	$53 \pm 6$	Ca I	$330 \pm 40$	Co I	$16 \pm 1$
C II	$(2.3 \pm 0.2)10^{-3}$	Al II	$0.36 \pm 0.05$	Ca II	$50 \pm 10$	Co II	0
C III	$(8.5 \pm 0.9)10^{-6}$	Al III	$12 \pm 1$	Ca III	...	Co III	$(4.0 \pm 2)10^{-7}$
N I	$(2.1 \pm 0.1)10^{-4}$	Si I	$6.0 \pm 0.6$	Sc I	$220 \pm 20$	Ni I	$26 \pm 2$
N II	$(7.5 \pm 0.5)10^{-6}$	Si II	$9 \pm 9$	Sc II	$(1.3 \pm 0.4)10^3$	Ni II	$(7.0 \pm 2.0)10^{-2}$
N III	$(7.0 \pm 1.0)10^{-6}$	Si III	$(5.8 \pm 0.6)10^{-4}$	Sc III	$(9.0 \pm 3.0)10^{-2}$	Ni III	$(3.0 \pm 2.0)10^{-7}$
O I	$(3.3 \pm 0.2)10^{-4}$	P I	$3.4 \pm 0.6$	Ti I	$97 \pm 5$	p <sup>c</sup>	$4.4 \times 10^{-11}$
O II	$(3.1 \pm 0.7)10^{-9}$	P II	$(2.2 \pm 0.3)10^{-3}$	Ti II	$28 \pm 2$	e <sup>c</sup>	0.27
O III	$(6.5 \pm 0.6)10^{-7}$	P III	$(5.0 \pm 2.0)10^{-4}$	Ti III	$(5.0 \pm 0.1)10^{-4}$	...	...

<sup>a</sup> $\beta = 0$  means that no ground state transitions are known in the range  $1\,000 \text{ \AA} < \lambda < 50\,000 \text{ \AA}$

<sup>b</sup>Empty entries mean that no atomic data are available

<sup>c</sup>Proton (H II) and electron values are calculated using Thomson cross section

spectral features are significantly broadened. A proper rotation of the spectrum requires detailed resolution of the photospheric absorption profiles, thus a special version of the model atmosphere was used in this work, which has constant spacing in wavelength, namely  $0.05 \text{ \AA}$  in the region  $1\,000\text{--}10\,000 \text{ \AA}$ , and  $0.5 \text{ \AA}$  in the region  $10\,000\text{--}50\,000 \text{ \AA}$  (P. Hauschildt & I. Kamp, private communication). A rotational broadening of this model spectrum was performed (e.g., Gray 1976), assuming a linear limb darkening law with  $\epsilon = 0.5$ . This choice adds an uncertainty in the relative flux level at the bottom of photospheric lines ranging from 2% in the visual to 10% in the UV. The spectrum was then flux calibrated using photometric information from the Tycho-2 Catalog (Høg et al. 2000) and the distance to the star. We estimate the error of this flux calibration to be  $\sim 4\%$ .

Table 1 shows the results of our calculations for elements from H to Ni. The mass of the star used is  $M = 1.75 M_{\odot}$  (Crifo et al. 1997). Calculation of uncertainties is explained in Appendix A. The agreement level with previously calculated values is highly variable. As an example, Lagrange et al. (1996) calculated  $\beta$  values using calibrated HST spectra. Our results agree with their values for Fe II, Al II and Al III within our uncertainties, but their result for Mg II differs from ours by a factor of 2. We take the good agreement between their Fe II value and ours as a consistency check, given the great number of transitions required to calculate  $\beta$  for this ion. Nevertheless, when looking at our results, it should be kept in mind that they were obtained with a generic model spectrum, therefore subject to possible systematic deviations from the particular  $\beta$  Pic case.

## 2.2. Ionization State of the Gas

Since we are interested in relating the dynamics of the gas to electrostatic interactions, we need to analyze in detail the ionization state of the gas. Given that the disk is optically thin, and the densities are low, the ionization state is determined by photoionization and radiative recombination. The temperature of the gas is below 300 K (Kamp & van Zadelhoff 2001), thus recombination rates are not very sensitive to the exact value of the temperature, depending most strongly on the electron density. Given the spectral type of the star (A5V), we expect most elements to be either singly ionized, or neutral.

We thus wrote a simple photoionization code which calculates the densities of neutral and ionized elements from H to Ni for an optically thin gas disk, with the corresponding electron density, and assuming solar composition. The latter choice is motivated by observations showing refractory elements having solar abundance relative to each other (Lagrange et al. 1995). The stellar ionizing radiation is obtained from our rotated and flux-calibrated model spectrum, whereas interstellar background UV field and and cosmic ray ionization rate ( $2 \times 10^{-17} \text{ s}^{-1} \text{ atom}^{-1}$ ) were taken from Weingartner & Draine (2001) and Spitzer (1978), respectively. Radiative recombination coefficients and photoionization cross sections were taken from the Cloudy C96.01 atomic data library (Ferland et al. 1998). Recombination of ions on dust grain surfaces, which can be the dominant recombination process in the interstellar medium, is not included as the dust in the disk is expected to have a *highly positive* charge (Appendix B), in contrast to the negatively charged grains of the interstellar medium.

At low temperatures the chemistry of the gas is not affected significantly if one sets  $T_{\text{gas}} = T_{\text{dust}}$  (Kamp & van Zadelhoff 2001), where  $T_{\text{gas}}$  is the gas temperature and  $T_{\text{dust}}$  is the dust temperature. We thus adopt a temperature profile corresponding to grains

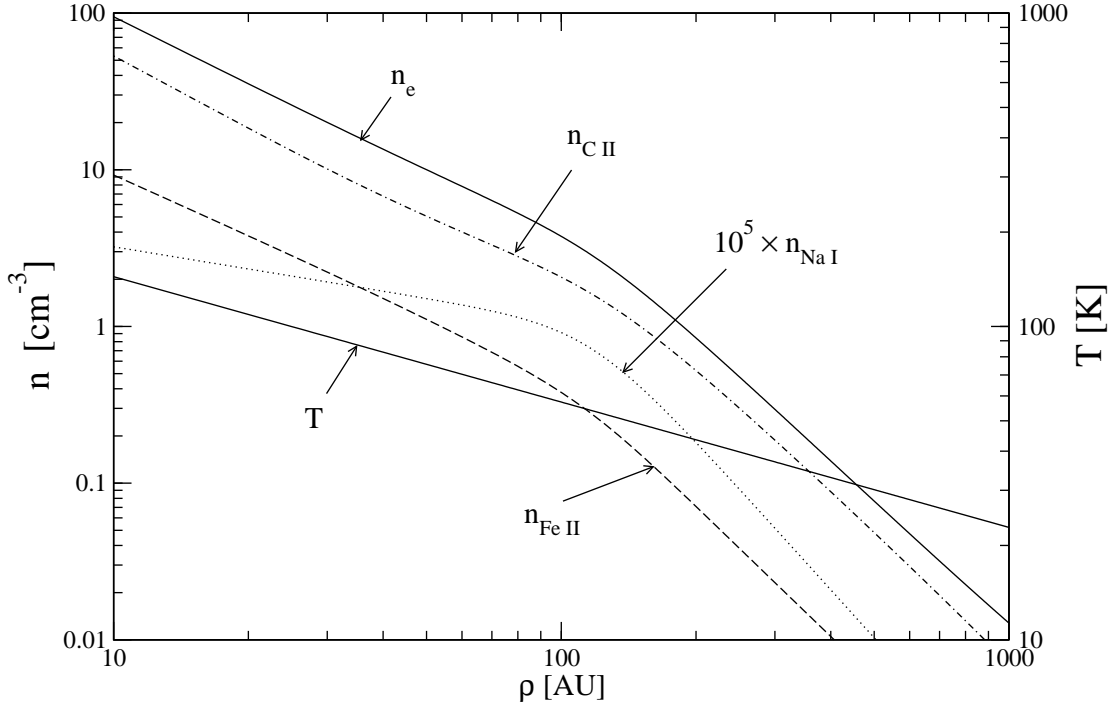


FIG. 1.— Plotted against cylindrical radius  $\rho$  are: average midplane dust temperature  $T$  (eq. 4, right axis), which we take to be the same as the local gas temperature; and midplane number densities (left axis) of electrons and selected species. Na I is obtained from observations (Brandeker et al. 2004), the remaining species are obtained from our photoionization code. C is partially ionized ( $\sim 50\%$ ) throughout the disk (and the main contributor of electrons), while Na and Fe are almost completely ionized.

of size  $a$  (e.g., Kamp & van Zadelhoff 2001)

$$T_a = 282.5 \left( \frac{L}{L_\odot} \right)^{1/5} \left( \frac{\text{AU}}{r} \right)^{2/5} \left( \frac{\mu\text{m}}{a} \right)^{1/5} \text{K}, \quad (3)$$

where  $L$  is the stellar luminosity ( $11 L_\odot$  for  $\beta$  Pic), and  $r$  is the distance to the star. To eliminate the dependence on grain size, we take a mean temperature weighted by grain surface area and size distribution

$$T_{\text{gas}}^4 = \langle T_a^4 \rangle = \frac{\int T_a^4 a^2 dn_a}{\int a^2 dn_a}. \quad (4)$$

We adopt  $dn_a \propto a^{-3.5}$  and perform the integral over the range  $a_{\min} < a < a_{\max}$ , with  $a_{\min} = 1 \mu\text{m}$  and  $a_{\max} = 1 \text{ km}$ . The chosen size distribution implies that the total grain surface area, and therefore our weighted temperature, is dominated by values corresponding to the smallest grains, being insensitive to the choice of  $a_{\max}$ . The resulting temperature profile in the disk midplane is shown in Figure 1 (right axis).

The observational constraint on the gas density comes from the fit to Na I emission (Brandeker et al. 2004), which has the form

$$n_{\text{Na I}}(\rho, z) = 10^{-5} \left[ \left( \frac{\rho}{\rho_0} \right)^{0.94} + \left( \frac{\rho}{\rho_0} \right)^{6.32} \right]^{-1/2} \exp \left[ - \left( \frac{z}{0.17\rho} \right)^2 \right] \text{cm}^{-3}, \quad (5)$$

where  $\rho$  is the distance to the star in the disk midplane,  $z$  the height above the midplane ( $r^2 = \rho^2 + z^2$ ), and  $\rho_0 = 117 \text{ AU}$ . The Na I profile in the disk midplane is shown in Figure 1, scaled by a factor  $10^5$ . Our photoionization code numerically solved for the densities of neutral and ionized species that are consistent with this Na I profile, the temperature profile of equation (4), and our assumption of solar composition. The sensitivity of our results to the adopted temperature profile is discussed in §4.1.

Our results show that H, He, N, O, F, Ne, and Ar, if present, are almost completely neutral, their marginal ionization ( $\sim 10^{-6}$ ) being determined by interstellar UV flux and cosmic rays. This group is unaffected by radiation force in its neutral phase. The elements C, Cl, Be, P, and S are partially ionized, with ionization fractions ranging from  $\sim 50\%$  for carbon to  $\gtrsim 95\%$  for beryllium.

TABLE 2  
VELOCITIES BEFORE IONIZATION FOR NEUTRAL  
SPECIES WITH  $\beta > 0.5$

Element	$\Gamma_{\text{star}}^{\text{a}}$ (s $^{-1}$ )	$v_{\text{ion}}^{\text{b}}$ (km s $^{-1}$ )	$n_{\text{I}}/n_{\text{II+}}^{\text{c}}$
Li I	$9.0 \times 10^{-6}$	0.11	$4.4 \times 10^{-6}$
Be I	$1.1 \times 10^{-9}$	58	$4.4 \times 10^{-2}$
B I	$7.5 \times 10^{-8}$	0.41	$6.1 \times 10^{-4}$
Na I <sup>d</sup>	$1.1 \times 10^{-7}$	3.3	$3.2 \times 10^{-4}$
Mg I	$6.8 \times 10^{-8}$	1.1	$6.4 \times 10^{-4}$
Al I	$1.1 \times 10^{-4}$	$5.0 \times 10^{-4}$	$8.5 \times 10^{-7}$
Si I	$3.9 \times 10^{-7}$	0.02	$1.3 \times 10^{-4}$
PI	$4.0 \times 10^{-10}$	8.7	$1.5 \times 10^{-1}$
SI	$4.0 \times 10^{-10}$	1.5	$6.4 \times 10^{-2}$
K I	$4.4 \times 10^{-7}$	0.5	$1.5 \times 10^{-4}$
Ca I	$1.3 \times 10^{-5}$	0.03	$3.5 \times 10^{-6}$
Sc I	$6.4 \times 10^{-8}$	3.5	$7.0 \times 10^{-4}$
Ti I	$1.5 \times 10^{-7}$	0.6	$3.0 \times 10^{-4}$
VI	$4.0 \times 10^{-7}$	0.2	$1.2 \times 10^{-4}$
Cr I	$1.0 \times 10^{-7}$	0.9	$4.8 \times 10^{-4}$
Mn I	$6.8 \times 10^{-8}$	0.4	$7.6 \times 10^{-4}$
Fe I <sup>d</sup>	$5.8 \times 10^{-8}$	0.5	$9.0 \times 10^{-4}$
Co I	$2.0 \times 10^{-8}$	0.8	$2.9 \times 10^{-3}$
Ni I <sup>d</sup>	$1.0 \times 10^{-7}$	0.3	$4.8 \times 10^{-4}$

<sup>a</sup>Stellar ionization rate at 100 AU from the star.

<sup>b</sup>Terminal velocity before ionization, *independent* of distance.

<sup>c</sup>Ratio of neutral (I) to ionized phase (II or higher) at  $r = 100$  AU in the disk midplane.

<sup>d</sup>Species with measured radial velocity by Brandeker et al. (2004) [see §2.2 for values and uncertainties]

Inside  $\sim 50$  AU the stellar ionization dominates, whereas UV background takes over at larger distances. While neutral carbon, chlorine, and sulfur feel little or no radiation pressure, the neutral phases of phosphorus and beryllium are accelerated. The potential of these species to trace the velocity of neutrals will be discussed below. The remaining species (including Na) are ionized to fractions  $\gtrsim 99.9\%$ . Electron densities in the disk midplane are shown in Figure 1, together with density profiles of C II and Fe II, which are the most abundant species by mass in the partially-, and heavily-ionized group.

The group with ionization  $\gtrsim 99.9\%$  contains all species affected strongly by radiation force. This is crucial for explaining the dynamics of the gas. From Table 1 we see that for most of these species, the highest  $\beta$  corresponds to the neutral phase (exceptions being Be and Sc), which has a very short lifetime compared to that of the ionized phase. Once ionized, elements feel a lower radiation force and can undergo Coulomb interactions with other charged particles and lose the excess momentum acquired from photons (§3.1).

A quantity of relevance is the velocity boost a neutral particle acquires before being ionized,  $v_{\text{ion}}$ . In the optically thin case, the ratio between the number per unit time of scattering photons to that of ionizing stellar photons depends only on the shape of the stellar spectrum, being *independent* of the distance to the star. The number of ionizing stellar photons hitting an atom per unit time is the stellar ionization rate

$$\Gamma_* = \int_0^\infty \frac{F_\lambda}{(hc/\lambda)} \sigma_{\text{ion}} d\lambda, \quad (6)$$

where  $\sigma_{\text{ion}}$  is the ionization cross section, the ionization time (or lifetime as neutral) being the inverse of  $\Gamma_*$ . The velocity boost before ionization is then

$$v_{\text{ion}} \simeq \beta \frac{GM}{r^2} \frac{1}{\Gamma_*}, \quad (7)$$

where  $\Gamma_*$  is evaluated at distance  $r$  from the star. Table 2 shows the results for elements with  $\beta > 0.5$ , for which the ionization rate due to interstellar UV is negligible relative to  $\Gamma_*$ . The most relevant feature is that, with the exception of Be I and PI, all neutrals feeling radiation force achieve velocities below 3.5 km s $^{-1}$  before being ionized. Since the acceleration in the neutral phase is nearly constant, the mean radial velocity is  $v_{\text{ion}}/2$ , provided no braking mechanism acts on particles in the neutral phase. This is consistent with observed values for neutrals:  $v_{\text{NaI}} = 1.2 \pm 0.3$  km s $^{-1}$ ,  $v_{\text{FeI}} = 0 \pm 0.3$  km s $^{-1}$ , and  $v_{\text{NiI}} = 0.4 \pm 0.4$  km s $^{-1}$  (Brandeker et al. 2004). Hence, as long as ionized particles are effectively braked, there is no need to find a braking mechanism for high- $\beta$  neutrals. Observed radial velocities of Be I and PI would be able to test these predictions. Unfortunately, their strongest ground state transitions are in the UV, which requires observations from space. The expected line equivalent widths, derived using our ionization model, would be 10 mÅ for PI  $\lambda 1774$ , while Be I  $\lambda 2350$  would be hardly detectable at 3  $\mu\text{A}$ .

### 3. BRAKING THE IONIC FLUID

We have established in the last section that the braking of neutral species is not required, only ions need to be slowed down. This changes the nature of the puzzle and makes it solvable. In this section we explore collisional processes involving electrostatic interactions that can account for the braking of ionized particles. From simple dynamical considerations it is clear that any braking medium needs to satisfy two requirements. First, a *high collision frequency* with ions, so that momentum can be effectively exchanged with particles accelerated by radiation. Second, the medium must provide a *high inertia*, so that it is not dragged along. We thus focus on three processes likely to operate in the disk: ion-ion, ion-dust, and ion-neutral collisions.

#### 3.1. Collisions between Ions

The fact that all the species affected by radiation pressure are highly ionized prompted us to explore first the role of Coulomb collisions among them. For treating the problem, we assume that magnetic fields are weak enough in the regions of interest,  $\sim 100$  AU from the star, so that the dynamics of charged particles is not influenced by them. Otherwise, complicated MHD effects may come into play. The statistical treatment of collisions among charged particles was studied by Spitzer (1956), based on results of Chandrasekhar (1941, 1943) for gravitational interactions. In Spitzer's framework, particles are categorized as *test* and *field* particles, the former having an initial velocity relative to the center of mass of the latter. Field particles are assumed to follow a Maxwellian velocity distribution. Braking of test particles is then characterized by the time it takes for the beam of test particles to diffuse in velocity space. This time corresponds to *dynamical friction* in the gravitational case, and is given by Spitzer (1956) as

$$t_S(t, f) = \frac{m_t^2(k_B T_f)v}{8\pi n_f Z_f^2 Z_t^2 e^4 (m_t + m_f) H(\xi) \ln \Lambda}, \quad (8)$$

where the subscripts t and f correspond to test and field particles, respectively. Here,  $v$  is the velocity of test particles relative to the center of mass of field particles,  $m$  is the mass of individual particles,  $n$  is the number density,  $Z$  is the charge in units of the electron charge  $e$  (throughout this work we assume  $Z_t = Z_f = 1$  for ions),  $T_f$  is the temperature of the field particles, and  $k_B$  is Boltzmann's constant. The quantities  $\xi$  and  $\Lambda$  are defined by

$$\xi = \frac{v}{c_{th,f}} \quad (9)$$

$$c_{th,f} = \sqrt{\frac{2k_B T_f}{m_f}} \quad (10)$$

$$\Lambda = \frac{\lambda_D}{b_{min}} = \frac{3}{2Z_f Z_t e^3} \left( \frac{k_B^3 T_e^3}{\pi n_e} \right)^{1/2}, \quad (11)$$

where  $c_{th,f}$  is the thermal velocity of field particles,  $\lambda_D$  is the electron Debye screening length,  $b_{min}$  is the minimum impact parameter for Coulomb collisions, and  $T_e$  is the electron temperature. In this context, electrons and ions are sufficiently thermalized to allow setting  $T_e = T_f$ . The  $\ln \Lambda$  factor accounts for the many weak scatterings out to distance  $\lambda_D$ . The functions  $H$  and  $\Phi$  are given by<sup>3</sup>

$$H(\xi) = \frac{\Phi(\xi) - \xi \Phi'(\xi)}{2\xi^2} \quad (12)$$

$$\Phi(\xi) = \frac{2}{\sqrt{\pi}} \int_0^\xi e^{-u^2} du. \quad (13)$$

Two related questions are considered here. First, for a newly ionized particle with speed  $v_{ion}$ , how long does it take to equalize its speed with the rest of the ions? Second, are high- $\beta$  ions dynamically coupled to low- $\beta$  ions?

The first question can be answered by evaluating  $t_S$  with the relative velocity  $v = v_{ion}$ , where  $v_{ion}$  is the velocity of neutral particles just before ionization, shown in Table 2. The resulting  $t_S$  in the disk midplane is shown in Figure 2 in units of the local Keplerian orbital period. It takes a very short amount of time for most newly ionized particles to be equalized with the ionic sea through Coulomb collisions, except for the element Be. A prediction is therefore that Be will be preferentially lost from the disk.

To address the second question, we express the timescale to radiatively accelerate a test ion as

$$t_{acc} = \frac{m_t v_*}{F_{rad}} = \frac{r^2 v_*}{(\beta_t - 1) GM}, \quad (14)$$

where  $v_*$  is the radial velocity relative to the star, and  $\beta_t > 1$  is the test particle radiation force coefficient. If  $t_S \ll t_{acc}$ , any excess momentum acquired by species that feel the radiation force will be transferred to the field particles as a result of many random collisions, the ions thus being dynamically coupled despite their different  $\beta$  values. Notice that the ratio  $t_S/t_{acc}$  does not depend on  $v$  except through the function  $H(\xi = v/c_{th,f})$ , which reaches a maximum when  $\xi \simeq 1$ . In Figure 3, we plot the ratio  $t_S/t_D$  as a function of the disk cylindrical coordinates  $\rho$  and  $z$ , taking  $\xi = 1$ , with C II as field particles and Fe II as test particles<sup>4</sup>. The species

<sup>3</sup> In (Spitzer 1956) the function in equation (12) is called  $G$ , but we rename it  $H$  to avoid confusion with the gravitational constant.

<sup>4</sup> When  $\xi \ll 1$  or  $\xi \gg 1$ ,  $t_S$  can become longer than  $t_{acc}$ . In the former case, ions may drift relative to each other, but with a speed orders of magnitude below the local sound speed.

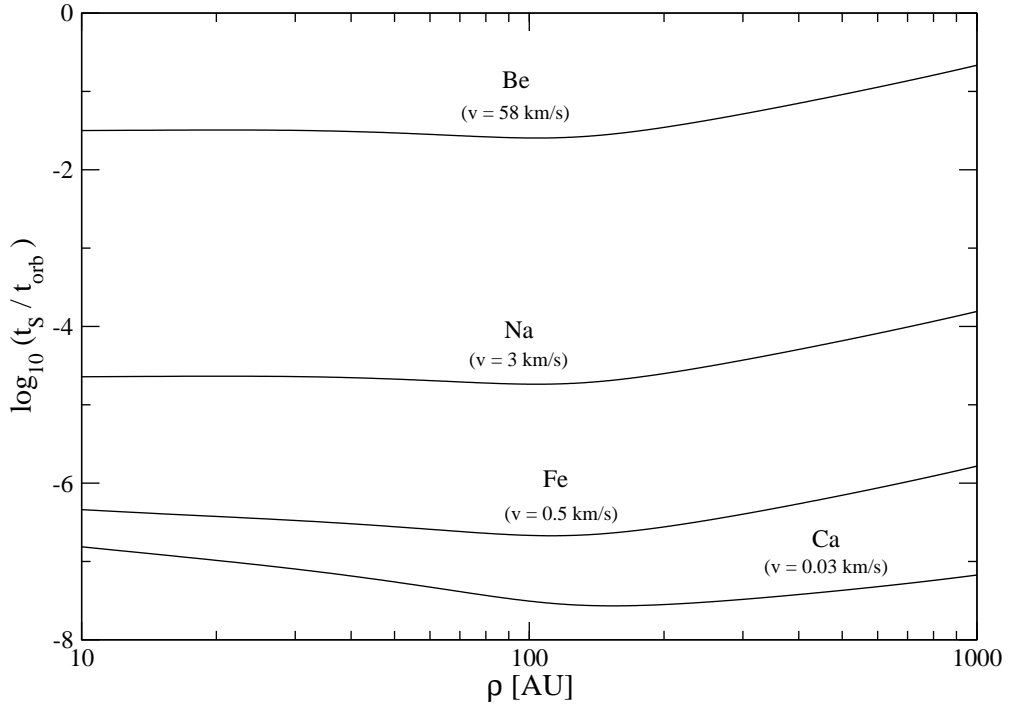


FIG. 2.— Ratio of slow-down to orbital timescales along the disk midplane, for ions with incident velocities  $v = v_{\text{ion}}$ , where  $v_{\text{ion}}$  is the velocity of neutral particles just before ionization, shown in Table 2. We adopt C II as field particles, but the results remain similar if other field particles are used.

chosen are representative as they are the most abundant (in number and mass) within groups that feel or do not feel radiation force ( $\beta_{\text{C II}} \approx 0$  and  $\beta_{\text{Fe II}} \approx 5$ , respectively).

Of particular interest is the coupling of ions at high altitudes over the midplane. Brandeker et al. (2004) detected Ca II emission being consistent with Keplerian orbits even at a height of  $z \sim 80$  AU ( $\rho \sim 120$  AU). In that zone we have  $t_s/t_{\text{acc}} \approx 0.05$  for  $v = c_{\text{th,f}}$ , i.e., ions are still coupled there. The effect of radiation force on the coupled ensemble of ions can be quantified by an effective radiation force coefficient

$$\beta_{\text{eff}} = \frac{\sum_j F_{\text{rad},j}}{\sum_j F_{\text{grav},j}} = \frac{\sum_j \beta_j \varrho_j}{\sum_j \varrho_j}, \quad (15)$$

where  $F_{\text{rad},j}$  and  $F_{\text{grav},j}$  are the radiative and gravitational forces acting on species  $j$  within a fluid element,  $\beta_j$  is the radiation pressure coefficient for species  $j$ , and  $\varrho_j$  is the mass density of species  $j$ . Thus  $\beta_{\text{eff}}$  is a weighted average of the values for each particle, the weight being the mass density of each species. If  $\beta_{\text{eff}} < 0.5$ , ions brake by themselves. Since ions outweigh electrons by a factor  $>2000$ , and there is one electron per ion, we neglect the electrons in the estimate of  $\beta_{\text{eff}}$  and assume that they are dragged along the ion fluid, preserving charge neutrality.

For solar composition, the most abundant ions by mass are, in decreasing order, C( $\beta \approx 0$ ), Fe(5), Si(9), Mg(9), S(0), Ni(0) and Ca(50). These particles dominate the value of  $\beta_{\text{eff}}$ , with carbon and iron being the relevant species. If all of them were 100% ionized, we would have  $\beta_{\text{eff}} \approx 3.5$ , but since the ionization fraction of C II varies with distance from the star, the actual value of  $\beta_{\text{eff}}$  is higher (by a factor 2 at most) and has a weak dependence on position. In Figure 4 we plot  $\beta_{\text{eff}}$  averaged over all ionized species as a function of disk cylindrical coordinates  $\rho$  and  $z$ . A straightforward way of braking the gas is by invoking an enhancement in the carbon abundance by a factor  $\sim 10$ . Observations of circumstellar absorption lines from C I and C II by FUSE, reported recently by Roberge et al. (2005), seem to indicate that carbon may indeed be over-abundant by this factor. Whether the gas is produced at this abundance or has evolved to it is, however, not clear at the moment. In the following sections we proceed to explore additional braking mechanisms that act independently of the relative abundance pattern of the gas.

### 3.2. Collisions with Charged Dust

Dust grains immersed in a plasma acquire a non-zero charge (Spitzer 1941), a phenomenon observed in the interstellar medium (ISM) and the solar system (e.g., Mendis & Rosenberg 1994, Horányi 1996). We therefore expect grains in the  $\beta$  Pic system to be charged as well. This might contribute to slow down the ion fluid by enhancing the ion-grain collision frequency relative to

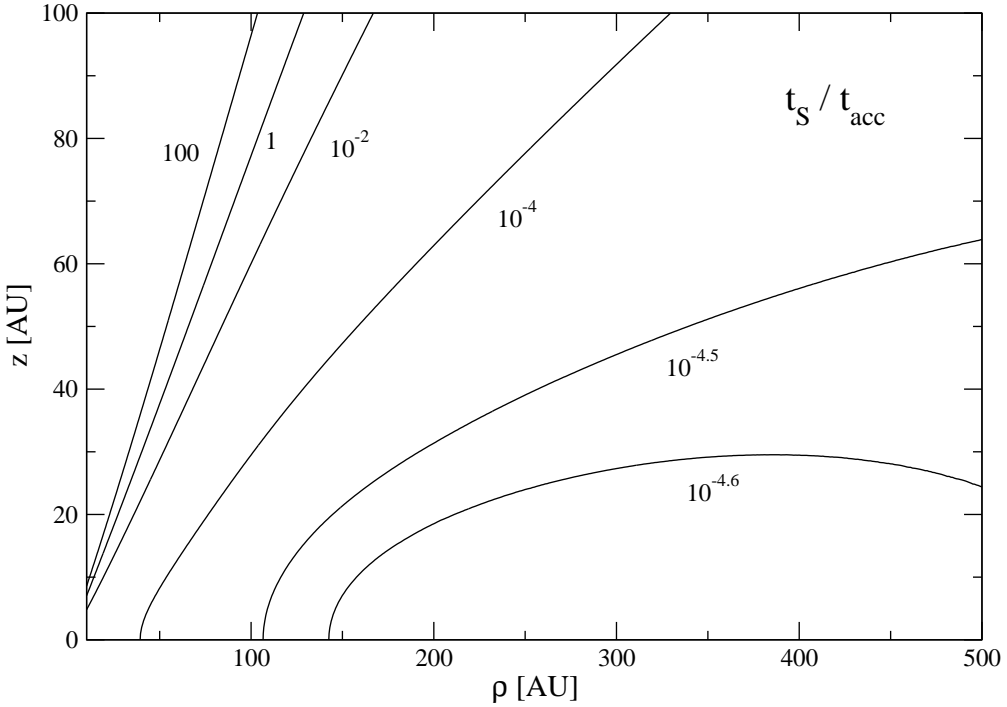


FIG. 3.— Contours of the ratio between the ion slow-down timescale and the radiative acceleration timescale (equations 8 and 14) in the  $\beta$  Pic disk ( $\rho$  and  $z$  are disk cylindrical coordinates). As an example, we adopt CII as field particles and FeII as test particles with injection velocity  $v = c_{\text{th,f}}$  ( $\xi = 1$ ). In regions of the disk where metallic gas has been observed, the ion slow-down time is orders of magnitude shorter than the radiative acceleration time, indicating that ions are dynamically coupled to a single fluid. Results are similar when we adopt other elements as field particles.

the case where grains are neutral. The mass in dust grains is expected to be larger than that of ionized particles, satisfying the requirement of high inertia. We therefore focus on the requirement of high collision frequency, which depends on the potential to which grains are charged to.

The relative importance of different grain charging mechanisms is determined by environment conditions (e.g., Mendis & Rosenberg 1994). In all cases, an equilibrium electrostatic potential is reached by balancing positive and negative currents. Given the spectral type of  $\beta$  Pic, and the fact that the disk is optically thin, the dominant source of positive charge is the ejection of photoelectrons by stellar UV radiation, while negative charge is provided by the collection of thermal electrons. The contribution of thermal ions and secondary electrons is negligible. As detailed in Appendix B, we solve for the equilibrium potential of grains in the  $\beta$  Pic disk given our model spectrum, temperature profile, and electron density (§§2.1 & 2.2). Due to the exponential fall-off of photon flux in the UV wavelengths, the potential depends weakly (in fact, logarithmically) on all variables except for the work function  $W$  of the grain (eq. B9). More detailed calculations yield that silicate dust ( $W = 8$  eV, Weingartner & Draine 2001) is charged to a positive potential  $e\phi \sim 0.2$  eV, while carbonaceous grains ( $W = 4.4$  eV, Weingartner & Draine 2001) achieve a much higher potential  $e\phi \sim 2.5$  eV, both values being fairly insensitive to the environment factors. High value for the latter group results from the fact that stellar photons with energy  $> 4.4$  eV are much more numerous than those above 8 eV. In any case, both potentials are much higher than  $\sim k_B T \sim 10^{-3}$  eV, the typical potential achieved when only thermal collection currents are included. Figure 5 shows the potential of silicates and carbonaceous grains normalized by  $k_B T$ , as a function of disk cylindrical coordinates. The contribution of the ejected photoelectrons to the ambient electron density is negligible, hence we did not couple grain charging with the ionization balance calculation.

Each dust grain is orders of magnitude more massive than a single ion, therefore grains can be considered to be immobile in space. As shown in §3.1, ions feel radiation force as an ensemble. They move with a velocity  $v$  relative to the grains, with an internal velocity dispersion  $c_{\text{th}}$  (equation 10). In a frame in which the center of mass of ions is at rest, dust grains drift with velocity  $-v$ . This relative motion is dissipated in a dynamical friction timescale (equation 8), with dust grains and ions as test and field particles, respectively. Since the frictional force felt by ions is equal and opposite to that felt by dust grains, the timescale for slowing down ions in the stellar frame is given by

$$t_{\text{id}} = \frac{\varrho_{\text{ion}}}{\varrho_{\text{dust}}} t_{\text{s}}(\text{dust, ion}) = \frac{m_{\text{ion}} k_B T v}{8\pi n_{\text{dust}} Z_{\text{dust}}^2 Z_{\text{ion}}^2 e^4 H(\xi) \ln \Lambda}, \quad (16)$$

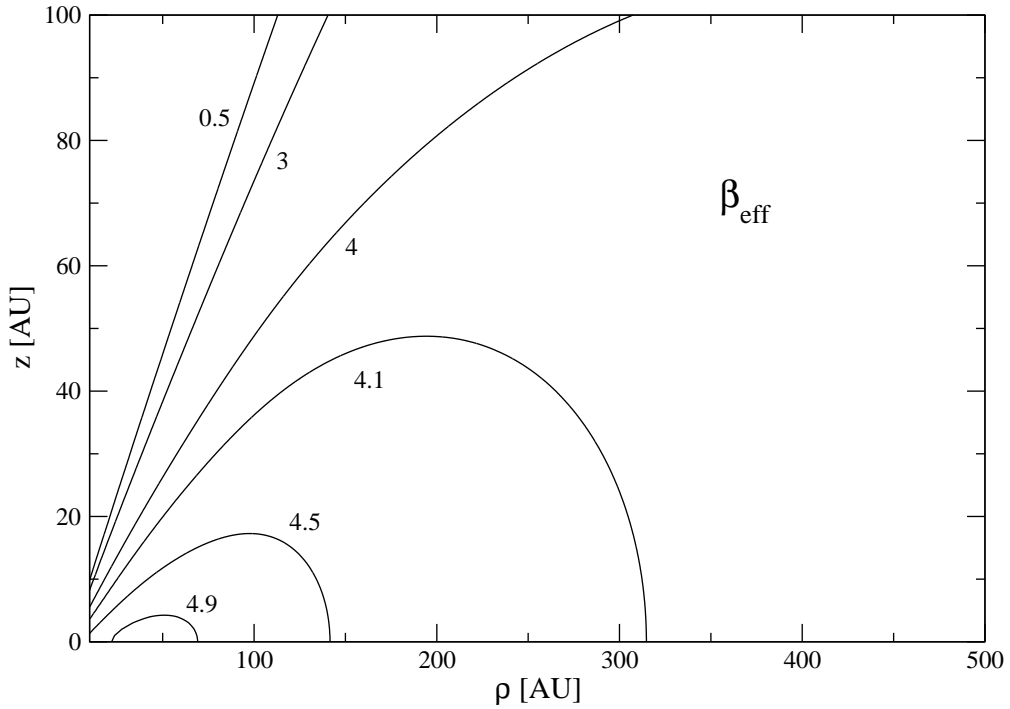


FIG. 4.— Contours of effective radiation pressure coefficient  $\beta_{\text{eff}}$  (equation 15), calculated by averaging the radiation force over all ionized particles, as a function of disk cylindrical coordinates  $\rho$  and  $z$ . Solar composition is assumed. Carbon, with  $\beta = 0$ , is important for reducing the value of  $\beta_{\text{eff}}$ . Increasing the ionization as one moves to larger distances (both outward and upward) accounts for the lowering of  $\beta_{\text{eff}}$ . However,  $\beta_{\text{eff}} > 0.5$  for all regions where metallic gas has been observed, indicating that an external agent is required to brake a solar-composition ionic fluid.

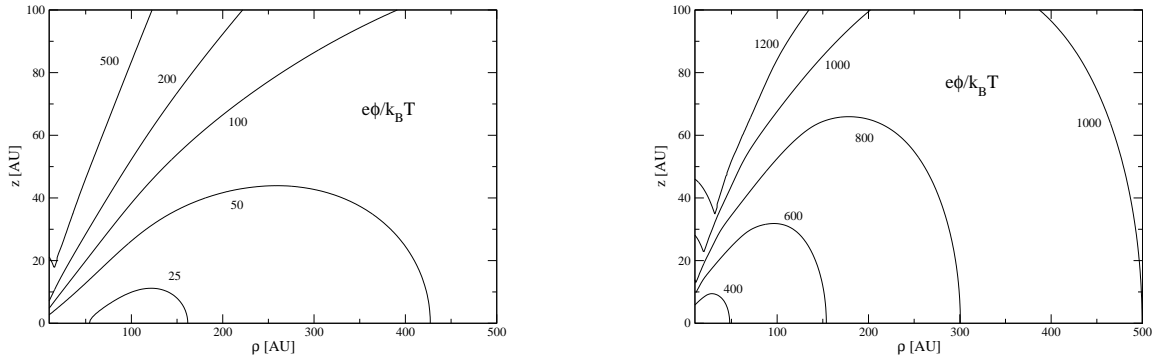


FIG. 5.— Equilibrium electrostatic potential of spherical grains  $e\phi$  (see Appendix B for details on the calculation) normalized by  $k_B T$ , as a function of disk cylindrical coordinates. Left panel shows silicates ( $W = 8$  eV) and right panel carbonaceous grains ( $W = 4.4$  eV). Due to strong photoelectric currents, both types of grains are charged to positive potentials much greater than  $\sim k_B T$ , the value expected if only thermal collection currents are responsible for charging grains. Results shown here are robust and depend only logarithmically on electron density, stellar luminosity, and orbital separation.

where  $\varrho_{\text{dust}}$  is the volume density of dust grains,  $\varrho_{\text{ion}}$  is that of ions, and the limit  $m_t \gg m_f$  was used in equation (8). The grain charge enters equation (16) through  $Z_{\text{dust}}$ . The dynamical friction timescale (equation 8) takes only into account the effect of distant encounters, i.e., impact parameters much larger than the grain size, under the assumption that the cumulative effect of these collisions outweighs that of close encounters (including impulsive ones) in determining the drag force (Spitzer 1956). Also, this expression does not include collective effects among ions (e.g., Northrop & Birmingham 1990). Both these effects are negligible for the following reasons. First, impact parameters are of order  $b \sim Z_{\text{dust}} e^2 / (k_B T)$ , thus most collisions are within

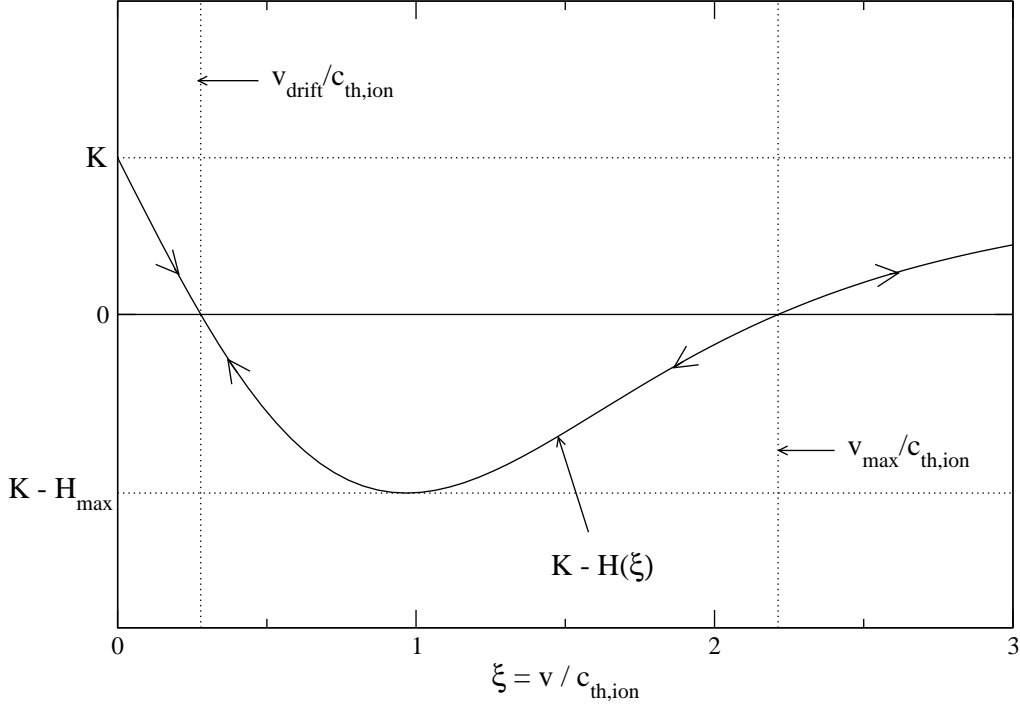


FIG. 6.— Function  $K - H(\xi)$  (equation 17), which determines the sign of the net force acting on an ion. Arrows indicate the stable and unstable nature of the equilibrium velocities  $v_{\text{drift}}$  and  $v_{\text{max}}$ , respectively. For any given value of  $K < H_{\text{max}}$ ,  $v_{\text{max}}$  is the maximum velocity for which braking can occur, whereas  $v_{\text{drift}}$  is the drift velocity that ions reach in a time  $t_{\text{id}}$  (equation 16).

the range  $a \ll b \ll \lambda_{\text{D}}$ , where  $a$  is the grain size and  $\lambda_{\text{D}}$  is the Debye screening length (consequently, we use  $b_{\text{min}} = a \simeq 1 \mu\text{m}$  in equation 11). Second, we have  $\omega_{\text{p}}a/c_{\text{th}} \sim 10^{-3}$ , where  $\omega_{\text{p}} = (4\pi n_{\text{e}}e^2/m_{\text{e}})^{1/2}$  is the electron plasma frequency, thus collective effects are not likely to contribute significantly to the drag force.

Under these assumptions, the equation of motion of a representative ion is given by

$$\begin{aligned} m_{\text{ion}} \frac{dv}{dt} &= (\beta_{\text{eff}} - 1) \frac{GMm_{\text{ion}}}{r^2} - \frac{m_{\text{ion}}v}{t_{\text{id}}} \\ &= (\beta_{\text{eff}} - 1) \frac{GMm_{\text{ion}}}{r^2} \left[ \frac{K - H(\xi)}{K} \right], \end{aligned} \quad (17)$$

where

$$K = \frac{(\beta_{\text{eff}} - 1)GMm_{\text{ion}}k_{\text{B}}T}{8\pi r^2 n_{\text{dust}} Z_{\text{dust}}^2 Z_{\text{ion}}^2 e^4 \ln \Lambda}. \quad (18)$$

The function  $H(\xi)$  is always positive, with a single maximum  $H_{\text{max}} \approx 0.2$  at  $\xi \approx 1$ , and asymptotic limits  $H(\xi) \sim 2\xi/(3\pi^{1/2})$  for  $\xi \ll 1$ , and  $H(\xi) \sim 1/(2\xi^2)$  for  $\xi \gg 1$ . Therefore, if  $K > H_{\text{max}}$ , no braking is possible, since the net force acting on an ion is always positive. In this case, as  $v$  increases, the relative contribution of the drag force decreases as  $1/v^2$ , leading to a runaway solution. If  $K < H_{\text{max}}$ , there exist two equilibrium velocities for which the net force on the ion vanishes, as shown in Figure 6. We denote them as  $v_{\text{max}}$  and  $v_{\text{drift}}$  ( $v_{\text{max}} > v_{\text{drift}}$ ). Ions with initial velocities  $v_{\text{drift}} < v < v_{\text{max}}$  will feel a drag force until they move with the velocity  $v_{\text{drift}}$  relative to the dust, while those with initial  $v > v_{\text{max}}$  will be accelerated outward without bound. These behaviors reflect the nature of charged dust braking.

We then calculate the value of  $K$  for the  $\beta$  Pic dust disk, taking  $m_{\text{ion}} = m_{\text{Fe}}$ ,  $Z_{\text{ion}} = 1$ , and  $Z_{\text{dust}}e^2/a = e\phi$ . The term  $n_{\text{dust}}a^2$  is understood to be summed over all grain sizes. As this term also appears in the dust optical cross section, its value can be obtained from fits to scattered and thermal emission (Artymowicz et al. 1989). In the present work we use an updated fitting formula for the dust profile, which assumes a constant grain albedo 0.5, and is based on HST observations of Heap et al. (2000)

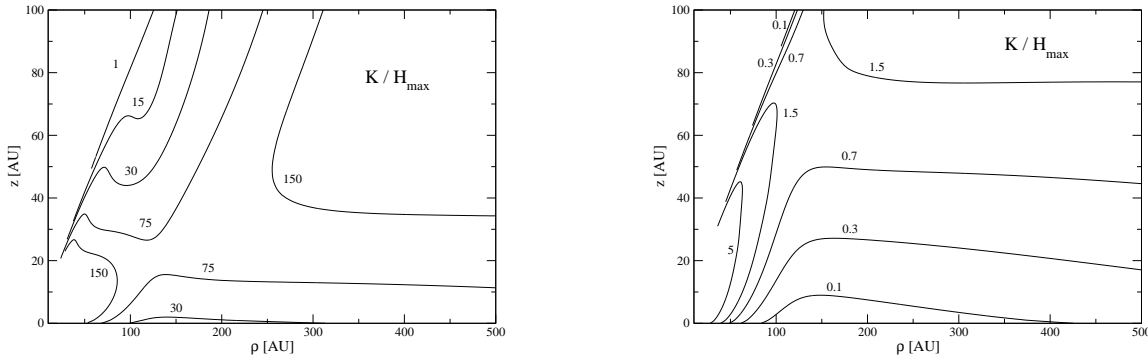


FIG. 7.— Constant  $K$  normalized by the maximum value of function  $H$  (equation 17) for 100% silicate (left) and 100% carbonaceous grains (right). Braking by charged dust requires  $K/H_{\max} < 1$ . While silicate grains are incapable of braking the ions, carbonaceous grains attain enough charge to exert a significant drag force and are thus an effective braking agent.

(P. Artymowicz, private communication):

$$\pi \langle a^2 \rangle n_{\text{dust}} = \frac{\tau_0}{W} \left[ \left( \frac{\rho}{\rho_0} \right)^{-4} + \left( \frac{\rho}{\rho_0} \right)^6 \right]^{-1/2} \exp \left[ - \left( \frac{z}{W} \right)^{0.7} \right], \quad (19)$$

with  $\rho_0 = 120$  AU,  $W = 6.6(\rho/\rho_0)^{0.75}$  AU, and  $\tau_0 = 2 \times 10^{-3}$ . The dust cross section (or differential optical depth) peaks at  $\sim 120$  AU, with an outward drop-off and an inner clearing region.

The resulting value of  $K$  as a function of disk cylindrical coordinates is shown in Figure 7 for 100% silicate (left) and 100% carbonaceous grains (right), normalized by  $H_{\max}$ . It can be seen immediately that silicates do not attain enough charge to make their interaction with ions significant. On the other hand, carbonaceous grains attain a much greater Coulomb cross section. Braking is most effective in the mid-plane region where dust density is the highest, the efficiency decreasing with increasing altitude above the midplane. However, at very high altitudes ( $z \geq 80$  AU and  $\rho \sim 100$  AU, roughly at the location where Ca II emission is detected), somewhat anti-intuitively, dust braking becomes effective again. This is explained by Figure 5, which shows increasing grain potential as altitude rises, a fact that is in turn explained by the exponentially decreasing electron density with altitude. If the disk is made of 100% carbonaceous grains, ions will be slowed down to velocities compatible with observational constraints, except very near the star ( $\rho \leq 50$  AU) where the dust density is too low. Figure 8 shows the corresponding values of  $v_{\text{drift}}$  and  $v_{\text{max}}$  for 100% carbonaceous grains.

Are dust grains expected to have a significant fraction of carbon? The answers seem to depend on the environment in which grains are found. For ISM grains, Weingartner & Draine (2001) deduced a combination of carbon and silicates, with carbon taking up  $\sim 35\%$  by volume, largely what one expects out of solar composition. Chondritic meteorites have only a few percent of carbon by volume, while most interplanetary dust particles collected in the Earth stratosphere are much more carbon rich, with  $> 50\%$  of carbon in some cases (Keller et al. 1994). Similar enrichment is found in comet Halley. It is thought that chondrites are relatively poor in volatiles because they have undergone some processing and are less primitive. Three pieces of work on  $\beta$  Pic may hold some clues to this question: albedo calculations (Artymowicz et al. 1989) suggest that dust in the outer disk is likely comprised of bright silicates (or ices) darkened by only a small amount ( $< 1\%$ ) of carbon materials;<sup>5</sup> silicate emission features are detected in the inner  $\beta$  Pic disk ( $< 20$  AU, Weinberger et al. 2003), though absent from the outer part; and a super-solar abundance for carbon in the gas phase is indicated by a UV absorption study (Roberge et al. 2005).

What are the constraints one can impose on the relative abundance of carbonaceous grains if they are solely responsible for braking the metallic gas? Braking requires  $K/H_{\max} < 1$  where  $K/H_{\max} \propto 1/n_{\text{dust}}$ . From Figure 7, we have  $K/H_{\max} \leq 0.1$  near the midplane region ( $z \leq 10$  AU) outside  $\rho > 100$  AU for the case of 100% carbonaceous grains. So for this region, a carbon fraction  $\sim 10\%$  is sufficient for braking. This fraction rises with altitude, inversely proportional to  $K/H_{\max}$ . We recall again that the dust density profile is still very uncertain, therefore these numbers should be taken as a very rough estimate.

### 3.3. Collisions with Neutral Gas

Collisions between neutral and ionized species have previously been investigated as a braking mechanism in the  $\beta$  Pic system (e.g., Beust et al. 1989; Lagrange et al. 1998). The dipole moment that ions induce on neutrals enhances the collision cross section relative to the neutral-neutral value (e.g., Beust et al. 1989). Previous studies, using neutral-neutral collisions and  $\beta$  values for neutral species, have estimated that  $\sim 50 M_{\oplus}$  of neutral gas are required to slow down elements affected by radiation force to within observational constraints (Brandeker et al. 2004). Here we perform a new estimate on the required mass to account for observations, using the fact that ions are dynamically coupled and are the only species feeling the radiation force.

<sup>5</sup> However, this result is based on a spatially unresolved SED. Revisiting the problem using resolved images (Heap et al. 2000) may yield new insights.

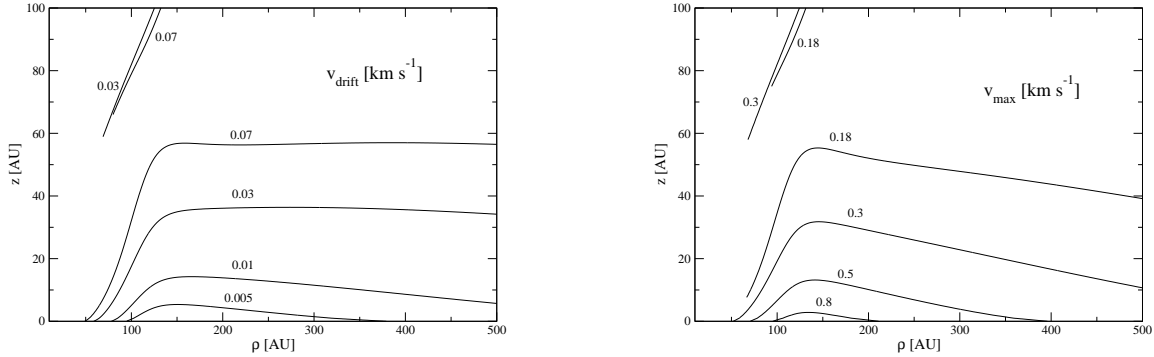


FIG. 8.—Drift velocity  $v_{\text{drift}}$  (left) and maximum velocity for braking  $v_{\text{max}}$  (right) for 100% carbonaceous grains, as a function of disk cylindrical coordinates. The value of  $v_{\text{drift}}$  falls below observational limits ( $\sim 1 \text{ km s}^{-1}$ ) in the majority of the disk.

Assuming that each ion-neutral collision absorbs  $m_n v_i$  momentum from ions, where  $m_n$  is the mass of neutral particles and  $v_i$  is the velocity of ions, the drag force exerted on an ion by neutrals is given by (e.g., Beust et al. 1989)

$$F_{\text{drag}} = -\varrho_n \pi \kappa v, \quad (20)$$

where, again, the subscripts  $i$  and  $n$  refer to ions (test) and neutral (field) particles, respectively,  $v$  is the relative velocity between the species, and  $\kappa$  is given by

$$\kappa = \sqrt{\frac{4\alpha_n Z_i e^2}{m_n}}, \quad (21)$$

where  $\alpha_n$  is the polarizability of neutral particles. Values of  $\alpha_n$  for several neutral atoms and molecules are shown in Table 3. The equation of motion for a representative ion is then

$$m_i \frac{dv}{dt} = (\beta_{\text{eff}} - 1) \frac{GMm_i}{r^2} - \varrho_n \pi \kappa v. \quad (22)$$

This has a single stable equilibrium solution when

$$v = v_{\text{drift}} = \frac{(\beta_{\text{eff}} - 1)GMm_i}{\pi \kappa \varrho_n r^2}. \quad (23)$$

Assuming that during the time  $t_{\text{drag}}$  it takes to slow down the ion, the distance it travels is much less than the distance to the star ( $v_{\text{drift}} t_{\text{drag}} \ll r$ ), the time dependent solution to (22) is given by (Liseau 2003)

$$v(t) \approx v_{\text{drift}} + (v_0 - v_{\text{drift}}) \exp(-t/t_{\text{drag}}), \quad (24)$$

where  $v_0$  is the initial relative velocity between the incident ion and the neutral gas, and

$$t_{\text{drag}} = \frac{m_i}{\pi \kappa \varrho_n} \quad (25)$$

is the characteristic timescale for momentum damping due to ion-neutral collisions.

Requiring a fixed drift velocity everywhere in the disk and integrating the required mass density (from equation 23) over a disk with vertical scale height  $H$ , we obtain a minimum mass for braking

$$\begin{aligned} M_{\text{min}} &= \frac{4GMm_i}{\kappa v_{\text{drift}}} \int_0^H \int_{\rho_{\text{min}}}^{\rho_{\text{max}}} \frac{(\beta_{\text{eff}} - 1)}{r^2} \rho d\rho dz \\ &= 3 \times 10^{-2} M_{\oplus} \left( \frac{m_n}{m_H} \right)^{1/2} \left( \frac{\alpha_{\text{HI}}}{\alpha_n} \right)^{1/2} \left( \frac{m_i}{m_{\text{Fe}}} \right) \left( \frac{0.1 \text{ km s}^{-1}}{v_{\text{drift}}} \right) \end{aligned} \quad (26)$$

where for numerical evaluation we have taken  $H = 100 \text{ AU}$ ,  $\rho_{\text{min}} = 10 \text{ AU}$ , and  $\rho_{\text{max}} = 1000 \text{ AU}$ . This result is much lower than previous estimates, for two reasons. First, since we are braking the ion ensemble, we have  $\beta_{\text{eff}} \sim 5$ , as opposed to individual species with  $\beta \sim 300$  (Na I, Ca I), requiring therefore less neutral material. Second, as only ions need to be braked, the collision frequency is enhanced relative to the neutral-neutral case due to induced dipole moment on the neutrals, the increase being of the same order as the reduction in the  $\beta$  value, further reducing the amount of braking material required to satisfy observational constraints. However, we note that since equation (26) assumes a constant drift velocity everywhere in the disk, the implied density profile  $\varrho_n \propto 1/r^2$  is unrealistic. Thus the value in equation (26) should be taken as a lower limit only.

TABLE 3  
POLARIZABILITIES FOR NEUTRAL ATOMS AND  
MOLECULES

Substance	$\alpha_n$ ( $10^{-24}$ cm $^3$ )	$\alpha_n/m_n$ ( $10^{-24}$ cm $^3$ mol g $^{-1}$ )
Experimental <sup>a</sup>		
H <sub>2</sub>	0.787	0.390
H <sub>2</sub> O	1.501	0.083
He	0.208	0.052
CO	1.953	0.070
Calculated <sup>b</sup>		
H	0.693	0.686
C	1.755	0.146
N	1.046	0.075
O	0.678	0.042

<sup>a</sup>Johnson (2005)

<sup>b</sup>Calculated using density functional B3LYP and basis set aug-cc-pVDZ (Johnson 2005)

Enforcing solar abundances everywhere in the disk, we can calculate the drift velocity using the density profile of §2.2, which implies a total disk mass of  $0.1 M_\odot$ . Figure 9 shows the value of  $v_{\text{drift}}$  as a function of disk cylindrical coordinates, assuming Fe II as test particles and HI as field particles. In most of the disk, this drift velocity is well below the observational constraints of Brandeker et al. (2004). However, in the zone corresponding to high-altitude Ca II emission ( $\rho \sim 120$  AU,  $z \sim 80$  AU) we have  $v_{\text{drift}} \approx 26$  km s $^{-1}$ , a factor 100 above what is observed. This discrepancy has two possible explanations: either our hydrogen profile falls off too steeply with height (due to, e.g., a wrong temperature), and/or the solar abundance assumption is not valid. The low temperatures in the outer regions of the  $\beta$  Pic disk allow for the existence of molecules (e.g., Kamp & van Zadelhoff 2001). A possible candidate for a braking medium could thus be water vapor sputtered from icy dust grains, which certainly does not need to follow solar abundance relative to the metallic gas. However, any braking medium other than hydrogen would require a higher total mass for a given drift velocity, since this element has the highest  $\alpha_n/m_n$  ratio and thus highest  $\kappa$ , as shown in Table 3. H<sub>2</sub>O, for instance, would need to be  $\sim 3$  times more massive to achieve the drift velocities in Figure 9.

Finally, we address the inertia requirement. Since the drag force on the ions is equal and opposite to the force exerted by the ions on the neutral gas, the requirement that the gravitational force on the latter is much larger than the force from the ions means  $(\beta_{\text{eff}} - 1)\varrho_i \ll \varrho_n$ , or  $\beta_{\text{eff}} M_{\text{ions}} \ll M_{\text{min}}$ . Using the results of §2.2, we obtain  $M_{\text{ions}} \approx 8 \times 10^{-4} M_\oplus$ , or  $M_{\text{min}} \approx 40 M_{\text{ions}} \sim 10\beta_{\text{eff}} M_{\text{ions}}$ , therefore the requirement of high inertia is satisfied even by the lower limit of equation (26). As mentioned before, any braking medium which follows a physical density profile is likely to have a mass higher than  $M_{\text{min}}$ .

#### 4. DISCUSSION

##### 4.1. Sensitivity to Gas Temperature

Our above results are obtained by assuming a thermal equilibrium between gas and dust. How reasonable is this and how sensitive are our results to this assumption?

Kamp & van Zadelhoff (2001) made a thorough study of the gas temperature in the  $\beta$  Pic disk, taking into account relevant heating and cooling mechanisms. They were able to set an upper limit  $\sim 300$  K for a solar composition gas, the major uncertainty being the unknown relative drift velocity between dust grains and gas particles, which they argue to be the dominant heating mechanism. Our study indicates that the gas disk can be significantly depleted in hydrogen relative to solar abundance. One naively expects that the gas will be cooler than the above upper limit, as cooling is dominated by line emissions from carbon and oxygen. This needs to be confirmed.

The observed gas disk has a finite thickness,  $h/r \sim 0.2$  at 100 AU (Brandeker et al. 2004). Assuming that this has a thermal origin (as opposed to a dynamical origin), and adopting a constant  $h/r$  ratio for the whole disk, we obtain a temperature profile

$$T \sim 9 \times 10^4 \text{ K} \left( \frac{m}{m_C} \right) \left( \frac{h/r}{0.2} \right)^2 \left( \frac{\text{AU}}{r} \right), \quad (27)$$

where  $m$  is the mean mass of a gas particle, and  $m_C$  that of a carbon atom. This yields  $T = 900$  K at  $r = 100$  AU, much hotter than the  $T = 60$  K value in the  $T_{\text{gas}} = T_{\text{dust}}$  approximation, and lies well above the upper limit of Kamp & van Zadelhoff (2001). This is puzzling and deserves further study.

Even adopting such a seemingly extreme temperature profile, we find that many of our conclusions remain unchanged. To reproduce the observed Na I density profile, the electron density at 100 AU rises slightly from  $n_e = 3.7$  cm $^{-3}$  to  $n_e = 5$  cm $^{-3}$ . The ionization balance depends on temperature weakly through the radiative recombination coefficients.<sup>6</sup> As a result, carbon, being intermediately ionized, is the only element that sees its ionization fraction changed significantly (rises from  $\sim 50\%$  to  $80-90\%$ ).

<sup>6</sup> Given the low gas densities, collisional ionization, charge exchange recombinations and dielectronic recombination are irrelevant for the ionization balance.

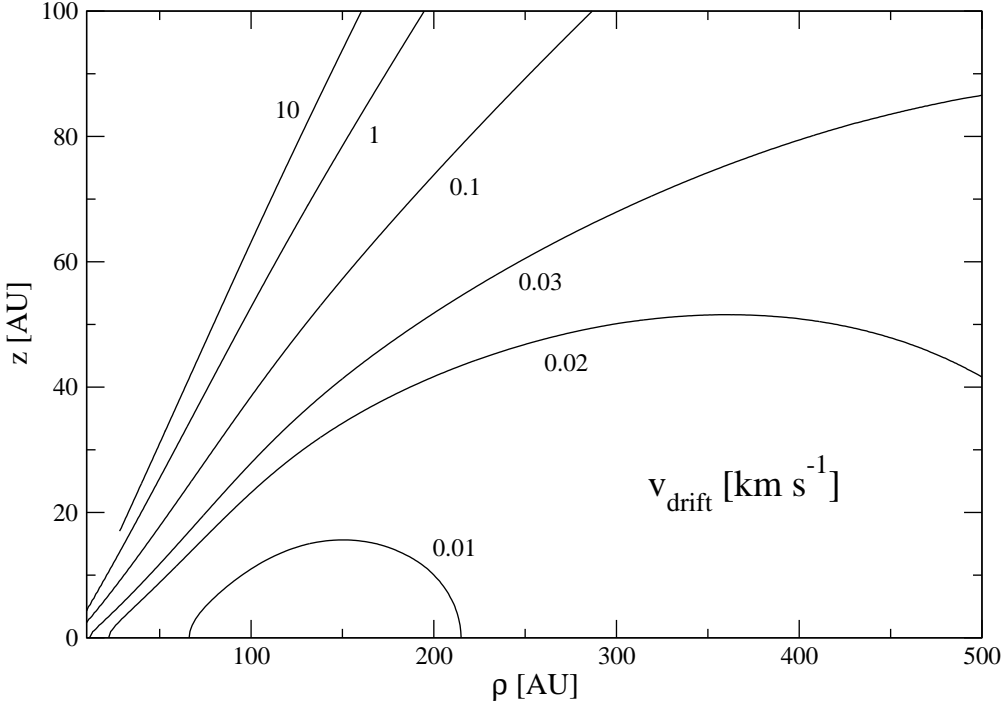


FIG. 9.— Magnitude of equilibrium drift velocity obtained by using the hydrogen density profile of §2.2 (for solar composition) and equation (23). This corresponds to a total gas mass of  $0.1 M_{\odot}$ . While metallic gas in the midplane region will drift slowly, satisfying observational constraints, the high-altitude regions where Ca II has been detected ( $\rho \sim 120$  AU and  $z \sim 80$  AU) is flowing outwards too fast.

This leads to a small decrease in the value of  $\beta_{\text{eff}}$  (more C II ions which do not see radiation pressure). The ratio  $t_S/t_{\text{acc}}$ , relevant for ion coupling, increases by about an order of magnitude: the linear dependence on  $k_B T$  in the numerator of equation (8) is softened by the increase in the ionized particles (mostly C II) and the slow increase of  $\ln \Lambda$ . Thus, coupling of ions remains efficient. The grain charge is mildly increased, as electron capture into grains is less efficient. However, the higher impact velocity increases the ratio  $K/H_{\text{max}}$  by a factor between 3 to 5. Dust braking becomes less effective, although carbonaceous dust remains capable of braking gas in the mid-plane. Braking by neutral gas is little affected by changes in temperature, with a weak indirect dependence via  $\beta_{\text{eff}}$ .

#### 4.2. Gas Origin and Lifetime

If either ion-grain or ion-neutral collisions are ultimately responsible for the slowing down of ions in the  $\beta$  Pic system, there is a finite drift velocity to which particles are slowed down. An estimate of the lifetime of the metallic gas can be obtained by calculating the time it takes for a single gas particle to travel the size of the disk  $R$  at a speed  $v_{\text{drift}}$ . For charged dust, assuming a 100% carbonaceous dust disk, we have

$$t_{\text{life}} \approx 2 \times 10^5 \left( \frac{m_{\text{ion}}}{m_{\text{Fe}}} \right)^{1/2} \left( \frac{60 \text{ K}}{T} \right)^{1/2} \left( \frac{0.1}{K/H_{\text{max}}} \right) \left( \frac{R}{300 \text{ AU}} \right) \text{ yr}, \quad (28)$$

whereas for ion-neutral collisions we have

$$t_{\text{life}} \approx 1.4 \times 10^4 \left( \frac{m_{\text{H}}}{m_{\text{f}}} \right)^{1/2} \left( \frac{\alpha_{\text{f}}}{\alpha_{\text{H}}} \right)^{1/2} \left( \frac{m_{\text{Fe}}}{m_{\text{t}}} \right) \left( \frac{R}{300 \text{ AU}} \right) \left( \frac{M_{\text{min}}}{3 \times 10^{-2} M_{\oplus}} \right) \text{ yr}. \quad (29)$$

One key question, important for constraints on gas evolution, is where the observed gas originates. Clues may be found in the observational evidence:

- (a) The metals observed in absorption follow *approximately* solar abundance (Lagrange et al. 1995).
- (b) There is a strong upper limit on the  $\text{H}_2$  column density in the disk from FUSE observations (Lecavelier des Etangs et al. 2001) that corresponds to a disk mass  $\sim 0.1 M_{\oplus}$ .

- (c) The metallic gas spatial distribution is very similar to that of the dust (Olofsson et al. 2001; Brandeker et al. 2004).
- (d) The metals observed in absorption and emission are close to rest relative to the star (Lagrange et al. 1998; Brandeker et al. 2004).

As to the origin of the observed metallic gas, we see three different possibilities:

1. The gas could be primordial, that is, a remnant from the initial cloud out of which the star formed. Equation (29) then implies a gas mass of  $30 M_{\oplus}$  to prevent the ions from leaving the system on a timescale shorter than the lifetime of the system,  $t_{\text{age}} \approx 10^7$  yr (Zuckerman et al. 2001). If the disk gas consists predominantly of hydrogen, then it would be in disagreement with (b). There remains the possibility that the gas disk is dominated by elements other than H, such as oxygen or oxygen-bearing molecules, which could have avoided detection. From an evolutionary point of view, however, it may be hard to justify why there should be such a large reservoir of oxygen left, and little hydrogen. Furthermore, the recent dynamical modeling of dust behavior in a gaseous disk by Thébault & Augereau (2005) excludes a gas disk more massive than  $\sim 0.4 M_{\oplus}$ .
2. The gas could be produced by bodies evaporating as they fall into the star, and then blown/diffused out by the radiation pressure to large distances in the disk (Lagrange et al. 1998). *Braking* gas could not be produced in such a scenario, since the gas would then just accumulate close to the release radius near the star. The hypothesis of remnant primordial gas braking the metallic ions from the inner disk faces a fine-tuning problem: with too little braking gas the metals will leave too quickly, whereas with too much braking gas the metals would never have reached the outer disk.

The production rate of gas required,  $\dot{M} = M_{\text{ion}}/t_{\text{life}} \sim 10^{-8} - 10^{-9} M_{\oplus} \text{ yr}^{-1}$ , is consistent with the production inferred from the FEB scenario (Lagrange-Henri et al. 1988). According to Thébault et al. (2003), this high evaporation rate is inconsistent with the structure of the inner dust disk around  $\beta$  Pic. A lower evaporation rate could still be consistent with the observed metallic gas density profile, provided that the drift velocity is decreased by the same amount by increasing the braking gas density. Constraint (b) limits the braking gas increase to a factor  $\lesssim 3$ .

If charged dust is primarily responsible for the gas braking, then (c) is a natural consequence of this. However, braking by dust is unlikely in this case. The main reason is that the gas is initially injected with a velocity  $\gg v_{\text{max}}$  (Figure 8), even in the favorable case of carbonaceous grains.

3. The gas could be created in grain-grain collisions, in line with the production of small dust grains from minor bodies (Thébault et al. 2003). The correlation between the dust and gas spatial distribution (c) would be a natural consequence of the production mechanism. Braking by dust is possible but not required, since even if the metallic ions are rapidly depleted initially, the neutral low- $\beta$  gas is left behind until the appropriate abundance pattern is reached for the ions to self-brake. If this is the case, then the gas volatiles are predicted to be somewhat enhanced relative to the metals, and at the same time deficient in H, since grains are expected to contain very little hydrogen.

If grains are able to brake ions, not only would the ions be tracing out the space distribution of smaller grains, they should also reveal the kinematics of dust. The near-Keplerian profile of metallic ions in the  $\beta$  Pic disk would therefore indicate that the grains, even at 300 AU, are still orbiting the star, raising the issue of how these grains get to these remote locations, since radiative blow out is not an option.

In summary, our results indicate that the hypothesis that the observed metallic gas is primordial can be excluded. We cannot rule out the possibility that the metallic gas is produced by falling evaporating bodies and then diffused outwards, but this requires coincidental circumstances that need a priori justification. We conclude that the gas is most likely produced by grain evaporation (possibly due to grain-grain collisions) and predict a gas composition where metals are depleted relative to the volatiles, and where the volatiles have the same relative abundance as in the grains.

#### 4.3. Extension to other systems

Given that several debris disks have been discovered around main sequence stars with different spectral types, we may ask whether the braking mechanisms we have studied so far are also important in those systems. We can do the simple exercise of calculating the radiation force coefficients, the ionization state, the value of  $\beta_{\text{eff}}$ , and attempt to draw some qualitative conclusions based on what we have learned in the previous sections. Table 4 shows radiation force coefficients and neutral fractions at  $r = 100$  AU in the midplane, as a function of spectral type, for C, Fe, Si, Mg, S, Ni, Ca, Al, Na, and K. The spectra are high resolution PHOENIX atmosphere models (P. Hauschildt, private communication) similar to those described in §2.1, flux calibrated and rotationally broadened according to the following stars: HR 4796A (A0V,  $3 M_{\odot}$ ,  $55 L_{\odot}$ ,  $v\sin i = 152 \text{ km s}^{-1}$ ), HD 107146 (G2V,  $1 M_{\odot}$ ,  $1 L_{\odot}$ ,  $200 \text{ km s}^{-1}$ ), TW Hya (K8V,  $0.6 M_{\odot}$ ,  $0.1 L_{\odot}$ ,  $5 \text{ km s}^{-1}$ ), and AU Mic (M1V,  $0.5 M_{\odot}$ ,  $0.05 L_{\odot}$ ,  $7 \text{ km s}^{-1}$ ). The ionization state for each case was obtained under the same constraints as the  $\beta$  Pic data (A5V,  $1.75 M_{\odot}$ ,  $11 L_{\odot}$ ,  $130 \text{ km s}^{-1}$ ), which is shown for comparison.

As expected, while  $\beta$  values decrease with later spectral type, neutral fractions increase. Spectral types G2, K8 and M1 have radiation force coefficients much smaller than 1, except for Na I and K I. These species are expected to be depleted in stars around K8, since they are mostly neutral, while still having  $\beta > 0.5$ . Late spectral types also have emission lines arising from chromospheric activity, which we do not account for in these calculations. This might increase the  $\beta$  values for the M1V type, making Na and K depletion more likely in these systems.

For the A0V case, all species are mostly in the ionized phase, but with higher  $\beta$  values than in  $\beta$  Pic. Using the densities of ionized species obtained by changing the spectral type to A0V, one obtains  $\beta_{\text{eff}} \approx 15$  at  $r = 100$  AU. This result should be taken

TABLE 4  
RADIATION FORCE, NEUTRAL FRACTIONS<sup>a</sup>, AND VELOCITIES BEFORE IONIZATION FOR DIFFERENT SPECTRAL TYPES

Type <sup>b</sup>	Quantity	C	Fe	Si	Mg	S	Ni	Ca	Al	Na	K
A0V	$\beta_I$	3	60	17	200	12	48	580	99	420	200
	$\beta_{II}$	0.1	21	25	40	0.01	0.5	180	20	0	0
	$n_I/n_{II+}$	0.01	3E-6	2E-7	6E-6	5E-4	5E-6	5E-7	1E-7	4E-5	3E-5
	$v_{ion} [\text{km s}^{-1}]$	2	5E-3	1E-4	0.04	0.02	6E-3	0.01	2E-4	0.06	0.1
A5V	$\beta_I$	0.03	27	6	74	0.6	26	330	53	360	200
	$\beta_{II}$	2E-3	5	9	9	9E-5	0.07	53	0.4	0	0
	$n_I/n_{II+}$	0.6	9E-4	1E-4	6E-4	0.06	5E-4	4E-6	9E-7	3E-4	2E-4
	$v_{ion} [\text{km s}^{-1}]$	...	0.5	0.02	1	2	0.3	0.03	5E-4	3	0.5
G2V	$\beta_I$	1E-5	0.06	4E-3	0.2	2E-5	0.1	3	0.3	12	26
	$\beta_{II}$	1E-7	7E-3	0.01	0.06	3E-8	2E-6	0.8	6E-5	0	0
	$n_I/n_{II+}$	0.6	0.9	0.06	2	0.2	2	6E-3	1E-3	0.08	0.03
	$v_{ion} [\text{km s}^{-1}]$	...	...	...	...	...	0.2	...	17	7	
K8V	$\beta_I$	6E-9	4E-3	4E-5	2E-3	3E-8	7E-3	0.2	0.02	3	11
	$\beta_{II}$	2E-11	2E-4	4E-5	2E-3	2E-	6E-8	0.06	3E-8	0	0
	$n_I/n_{II+}$	0.7	1	0.07	3	0.2	3	0.5	0.1	14	13
	$v_{ion} [\text{km s}^{-1}]$	...	...	...	...	...	...	...	9E+3	2E+3	
M1V	$\beta_I$	7E-10	5E-4	6E-6	4E-4	8E-9	7E-4	0.04	2E-3	0.6	2.1
	$\beta_{II}$	4E-12	2E-5	7E-6	2E-4	6E-10	2E-8	0.01	3E-9	0	0
	$n_I/n_{II+}$	0.7	1	0.07	3	0.2	3	0.6	0.1	15	20
	$v_{ion} [\text{km s}^{-1}]$	...	...	...	...	...	...	...	1E+4	2E+3	

<sup>a</sup>Neutral fractions were computed at  $r = 100$  AU in the disk midplane, under the same constraints as the values determined in §2.2 for  $\beta$  Pic, changing only the spectrum.

<sup>b</sup>Corresponding to model spectra (see text for details), flux calibrated and rotationally broadened according to particular cases (see text). No chromospheric emission was included in the model.

only as a rough reference, since ionization fractions depend on the densities of different species, which in turn depend on disk mass and composition.

Also shown are velocities before ionization  $v_{ion}$  calculated as in equation (7), which have a physical meaning only when  $\beta > 0.5$  (when  $\beta < 0.5$ , the species feels a gravitational attraction weaker by a factor  $[1 - \beta]$ , but is still bound to the star). Again, Na and K seem to be the problem, being likely decoupled from the rest of the ions in the G2 disk, in the same way as Be is decoupled in  $\beta$  Pic (§2.2). Ions are likely to be very strongly coupled for the A0 case.

## 5. CONCLUSIONS

Motivated by the apparent contradiction between the strong radiation force acting on the gas in the  $\beta$  Pictoris disk and spatially resolved observations showing it to be consistent with Keplerian rotation, we have explored different braking mechanisms that are likely to operate in the disk. We have found that:

- a) All species affected strongly by radiation force are heavily ionized. The velocities that the short-lived neutral particles achieve as a result of radiative acceleration, before becoming ionized, are consistent with observational constraints.
- b) Ions are dynamically coupled due to their high Coulomb collision frequency. They feel a single effective radiation force coefficient  $\beta_{eff}$ . For solar composition, this coefficient is  $\sim 5$ , in which case ions cannot brake by themselves. If carbon is over-abundant by a factor  $\gtrsim 10$  on the other hand, the ion fluid may indeed be self-braking.
- c) If a significant fraction of the dust in the disk is carbonaceous, the ion ensemble can be slowed down to drift velocities below the local sound speed by photoelectrically charged dust grains. This fraction is as low as 10% near the midplane and rises with altitude above the midplane.
- d) Ions can also be slowed down by collisions with neutral gas (e.g.,  $H_2$ ,  $H_2O$ ). The amount of neutral material required to satisfy observational constraints on drift velocities is  $< 1 M_\oplus$ , substantially less than previous estimates. The UV absorption upper limit on  $H_2$  is  $\sim 0.1 M_\oplus$  (Lecavelier des Etangs et al. 2001).
- e) Reasonable assumptions on gas drift velocities imply gas lifetimes of order  $10^4 - 10^5$  yr, much lower than the age of the system and which require a replenishment mechanism, in analogy with the dust.

The required gas production rate  $10^{-13} M_\odot \text{ yr}^{-1}$  is comparable to the FEB scenario prediction (e.g., Lagrange-Henri et al. 1988), although we argue that gas is more likely to be produced by local dust grain evaporation. A primordial origin of the gas is ruled out, since for having a lifetime of  $\sim 10^7$  yr it would require a substantial quantity of neutral material, which would have already been detected.

Further gas observations in this and other systems would be able to test several predictions arising from this work, such as the absence of P and Be in  $\beta$  Pic, and the relative importance of ion-grain and ion-neutral collisions for slowing down ions. A more detailed study of the dust composition would shed light on the feasibility of the dust braking scenario.

We are grateful to Peter Hauschildt and Inga Kamp for making the high-resolution model spectra available to us. We also thank useful discussions with Norm Murray, Paweł Artymowicz, Chris Matzner, Peter Goldreich, Yuri Levin, René Liseau, Per Carlqvist, Hilding Neilson, and Amr El-Zant. Comments by an anonymous referee were helpful for improving this paper. We acknowledge financial support from NSERC. This work made extensive use of NASA's Astrophysics Data System.

## APPENDIX

### UNCERTAINTIES IN THE RADIATION FORCE COEFFICIENTS

The errors in the radiation force coefficients being quoted in Table 1 were calculated using the following expression:

$$\left(\frac{\delta\beta}{\beta}\right)^2 = \left(\frac{\delta F}{F}\right)_{\text{cal}}^2 + \frac{1}{\beta^2} \sum_i \left(\frac{g_0}{\sum g_0}\right)^2 \beta_i^2 \left[ \left(\frac{\delta A_{i0}}{A_{i0}}\right)^2 + \left(\frac{\delta F}{F}\right)_{\text{limb},i}^2 \right] \quad (\text{A1})$$

where  $\delta\beta$  is the error quoted in Table 1,  $\beta_i$  and  $\delta A_{i0}$  are the radiation force coefficient and error in Einstein coefficient corresponding to the  $i$ -th transition, respectively,  $(\delta F/F)_{\text{limb},i}$  is the fractional error in the stellar flux (at the given transition) due to uncertain limb darkening used in the rotational broadening of the spectrum, and  $(\delta F/F)_{\text{cal}}$  is the fractional uncertainty in the overall flux calibration. The term  $(g_0/\sum g_0)$  represents the weighted average between different multiplets of ground states, when applicable (e.g., Fe I), where it is assumed that the population of a multiplet is proportional to its statistical weight.

Values for  $(\delta A/A)$  range from 3% for the stronger transitions, to more than 50% for the weaker ones (Martin et al. 1999). The factor  $(\delta F/F)_{\text{limb},i}$  was estimated by rotating the atmosphere model with limb darkening coefficients  $\varepsilon = \{0, 0.5, 1\}$  and calculating the fractional deviation, as a function of wavelength, relative to the  $\varepsilon = 0.5$  case. As mentioned in the main text, the error  $(\delta F/F)_{\text{cal}}$  was estimated to be 4%, although systematic deviations may arise between the generic model spectrum and the particular  $\beta$  Pic case.

### GRAIN CHARGING IN THE $\beta$ PIC DISK

The relative importance of different grain charging mechanisms is determined by four parameters: the dust grain size  $a$ , the Debye screening length  $\lambda_D$  of electrons, the mean intergrain separation  $n_d^{-1/3}$ , and the UV flux incident on the system (Mendis & Rosenberg 1994). A lower limit on the intergrain separation can be estimated by using the smallest grain size and the highest dust mass in the disk. Assuming a higher limit for dust mass  $\sim 120 M_\oplus$  in the disk (Artymowicz 1997), using the smallest grain size  $a \sim 1 \mu\text{m}$  (Backman & Paresce 1993), grain mass density  $\sim 1 \text{ g cm}^{-3}$ , and a disk volume  $\pi(100 \text{ AU})^2 \times (10 \text{ AU})$  we estimate  $n_d^{-1/3} \gtrsim 180 \text{ cm}$ . Using the results of §2.2, we get  $\lambda_D \approx 10\text{--}80 \text{ cm}$ . Thus, the  $\beta$  Pic disk is in the regime  $a < \lambda_D < n_d^{-1/3}$ , where grains can be treated as isolated particles immersed in an ionized gas, i.e., collective effects of charged grains play no role (Mendis & Rosenberg 1994).

The equilibrium electrostatic potential of a grain  $\phi$  is found by balancing all the currents that charge the grain. Given the UV flux of the star, photoelectric charging is the dominant process, with a current per unit area given by (e.g., Draine 1978)

$$J_{\text{ph}} = \frac{e}{4} \int_{(e\phi+W)/h}^{\nu_{\text{max}}} \left[ \int_{e\phi}^{h\nu-W} f(E, h\nu) dE \right] Q_{\text{abs}}(\nu) Y(h\nu) \frac{F_\nu}{h\nu} d\nu \quad (\text{B1})$$

for the case of spherical grains with  $\phi > 0$ . Here,  $F_\nu$  is the stellar flux per unit frequency,  $Q_{\text{abs}}$  the grain absorption efficiency,  $Y$  the photoelectric yield,  $W$  the grain work function, and

$$f(E, h\nu) = \frac{6}{h\nu - W} \left( \frac{E}{h\nu - W} \right) \left( 1 - \frac{E}{h\nu - W} \right) \quad (\text{B2})$$

is the photoelectron kinetic energy distribution function, which we approximate as a parabolic function (e.g., Weingartner & Draine 2001). The integral over electron energy is then

$$\int_{e\phi}^{h\nu-W} f(E, h\nu) dE = 1 - 3 \left( \frac{e\phi}{h\nu - W} \right)^2 + 2 \left( \frac{e\phi}{h\nu - W} \right)^3. \quad (\text{B3})$$

The photoelectric yield is approximated as (Draine 1978)

$$Y(h\nu) = \frac{1}{2} \left( 1 - \frac{W}{h\nu} \right). \quad (\text{B4})$$

The fact that the grains in the disk have a minimum size of order  $\sim 1 \mu\text{m}$  (Backman & Paresce 1993) allows the use of work functions corresponding to bulk matter. The values adopted are  $W = 8 \text{ eV}$  for silicates and  $W = 4.4 \text{ eV}$  for carbonaceous grains (Weingartner & Draine 2001). The minimum size of the grains also justifies taking the absorption efficiency for UV radiation as  $Q_{\text{abs}}(\nu) = 1$  (e.g., Greenberg 1971).

The positive photoelectric current in equation (B1) is balanced by a thermal electron collection current per unit area (e.g., Spitzer 1941):

$$J_e = -es_e n_e \sqrt{\frac{k_B T_e}{2\pi m_e}} \left( 1 + \frac{e\phi}{k_B T_e} \right), \quad (\text{B5})$$

where we use a sticking coefficient  $s_e = 0.5$  (Draine 1978). Given the low temperature of the gas, the incident electrons have energies  $\ll 1$  eV, not enough to make secondary electron emission important (e.g., Mendis & Rosenberg 1994). The ion counterpart to equation (B5) is found to be negligible, since these particles are strongly repelled when  $e\phi > 0$  (e.g., Spitzer 1941). Provided that relative drift velocities between dust grains and electrons are smaller than the electron thermal velocity (i.e.,  $v \lesssim 40$  km s $^{-1}$ ), it is not necessary to correct equation (B5) for this effect (Northrop & Birmingham 1996), since positive charge is not provided by ions but by photoelectrons. We set  $T_e$  equal to the gas temperature  $T$ , equation (4).

The equilibrium grain potential is found by solving  $J_{ph} - J_e = 0$ , the result being shown in Figure 5, normalized by the local value of  $k_B T$ . As mentioned in the main text, the contribution of the ejected photoelectrons to the ambient electron density is very small. We estimate an upper limit to the density of ejected photoelectrons as

$$n_{e,dust} \leq \left( \frac{e\phi}{k_B T} \right) \frac{ak_B T}{e^2 \lambda_D^3} \sim 0.2 \text{ cm}^{-3} \ll n_e \quad (\text{B6})$$

for  $e\phi/(k_B T) = 1000$ ,  $T = 60$  K,  $n_e = 4$  cm $^{-3}$ , and  $a = 1$   $\mu$ m. In the following, we provide a rough estimate for the equilibrium potential, and show that it depends strongly on the grain work function ( $W$ ), but logarithmically on all other parameters, making our results quite robust.

In the Wien regime, photon flux can be approximated as

$$F_\nu = f_0 \left( \frac{\text{AU}}{r} \right)^2 \nu^3 \exp \left( -\frac{h\nu}{k_B T_*} \right), \quad (\text{B7})$$

where  $k_B T_* \approx 0.7$  eV for  $\beta$  Pic,  $r$  is the distance to the star, and  $f_0 = F_\nu(\nu_0) \exp(h\nu_0/[k_B T_*])/\nu_0^3$ , with  $F_\nu(\nu_0) \approx 3 \times 10^{-9}$  erg cm $^{-2}$  s $^{-1}$  Hz $^{-1}$  and  $h\nu_0 = 4.4$  eV. We integrate the photoelectric current (equation B1) taking only account of the exponential drop-off in the flux (and disregarding factors of order unity outside the exponential factor),

$$J_{ph} \sim \frac{e}{8} \left[ \left( \frac{\text{AU}}{r} \right)^2 \frac{f_0 \nu^3}{h} \frac{k_B T_*}{h\nu} \right]_{h\nu \approx e\phi+W} \exp \left( -\frac{e\phi+W}{k_B T_*} \right) \sim \left[ \left( \frac{\text{AU}}{r} \right)^2 \frac{f_0 W^2 k_B T_*}{h^4} \right] \exp \left( -\frac{e\phi+W}{k_B T_*} \right) \quad (\text{B8})$$

where we have used the fact that  $W \geq e\phi$ . Even if this may not be a good approximation, the current depends exponentially on the ratio  $(e\phi+W)/k_B T_*$  and other factors outside the exponential matter little. We also simplify the equation (B5) by assuming  $e\phi \sim k_B T_* \gg k_B T$ . We equate the above expression to the photoelectric current, and solve for the equilibrium potential:

$$e\phi = k_B T_* \ln \left[ \frac{1}{8s_e n_e} \left( \frac{\text{AU}}{r} \right)^2 \left( \frac{f_0 W^2 k_B T_*}{h^4} \right) \sqrt{\frac{2\pi m_e}{k_B T}} \frac{T}{T_*} \right] - W \quad (\text{B9})$$

This shows that the charging potential depends on all environment variables logarithmically, and is only affected strongly by the work function. Substituting in our fiducial values ( $r = 100$  AU,  $n_e \sim 4$  cm $^{-3}$ ,  $s_e = 0.5$ ,  $T = 60$  K) for the  $\beta$  Pic disk, we obtain  $e\phi \sim 2.8$  eV for silicate dust ( $W = 8$  eV) and  $e\phi \sim 5.5$  eV for carbon dust ( $W = 4.4$  eV). Both values are much greater than the values one expects if photoelectric charging is absent ( $e\phi \sim k_B T \sim 10^{-3}$  eV). We numerically calculate these potentials (Fig. 5) using a realistic stellar spectrum and found them to be somewhat smaller than the values obtained here.

## REFERENCES

Artymowicz, P. 1997, *Annu. Rev. Earth Planet. Sci.*, 25, 175

Artymowicz, P., Burrows, C., & Paresce, F. 1989, *ApJ*, 337, 494

Aumann, H. H., et al. 1985, *ApJ*, 278, L23

Backman, D. E., & Paresce, F. 1993, in *Protostars and Planets III*, ed. E. H. Levy, & J. I. Lunine (Tucson: Univ. Arizona Press), 1253

Beust, H., Lagrange-Henri, A. M., Vidal-Madjar, A., & Ferlet, R. 1989, *A&A*, 223, 304

Bodenheimer, P., & Lin, D. N. C. 2002, *Annu. Rev. Planet. Sci.*, 30, 113

Brandeker, A. 2004, PhD Thesis, Stockholm University, available from the author on request

Brandeker, A., Liseau, R., Olofsson, G., & Fridlund, M. 2004, *A&A*, 413, 681

Chandrasekhar, S. 1941, *ApJ*, 93, 285

Chandrasekhar, S. 1943, *ApJ*, 97, 255

Crifo, F., Vidal-Madjar, A., Lallement, R., Ferlet, R., & Gerbaldi, M. 1997, *A&A*, 320, L29

Draine, B. T. 1978, *ApJS*, 36, 595

Ferland, G. J., Korista, K. T., Verner, D. A., Ferguson, J. W., Kingdon, J. B., & Verner, E. M. 1998, *PASP*, 110, 761

Ferlet, R., Hobbs, L. M., & Vidal-Madjar, A. 1987, *A&A*, 185, 267

Freudling, W., Lagrange, A.-M., Vidal-Madjar, A., Ferlet, R., & Forveille, T. 1995, *A&A*, 301, 231

Gray, D. F. 1976, *The Observation and Analysis of Stellar Photospheres*, (New York: Wiley)

Greenberg, J. M. 1971, *A&A*, 12, 240

Hauschildt, P. H., Allard, F., & Baron, E. 1999, *ApJ*, 512, 377

Heap, S. R., Lindler, D. J., Lanz, T. M., Cornett, R. H., Hubeny, I., Maran, S. P., & Woodgate, B. 2000, *ApJ*, 539, 435

Hilborn, R. C. 1982, *Am. J. Phys.*, 50, 982

Hobbs, L. M., Vidal-Madjar, A., Ferlet, R., Albert, C. E., & Gry, C. 1985, *ApJ*, 293, L29

Høg, E., et al. 2000, *A&A*, 335, L27

Horányi, M. 1996, *ARA&A*, 34, 383

Johnson, R. D. (ed.) 2005, *NIST Computational Chemistry Comparison and Benchmark Database, NIST Standard Reference Database Number 101*, (Gaithersburg, MD: NIST), Release 11, <http://srdata.nist.gov/ccbdb>

Kamp, I., & Zadelhoff, G.-J. 2001, *A&A*, 373, 641

Keller, L. P., Thomas, K. L., & McKay, D. S. in *Carbon in Primitive Interplanetary Dust Particles*, ed. E. Zolensky, T. L. Wilson, F. J. M. Rietmeijer, & G. J. Flynn (New York: AIP), 159

Lagage, P. O., & Pantin, E. 1994, *Nature*, 369, 628

Lagrange-Henri, A. M., Vidal-Madjar, A., & Ferlet, R. 1988, *A&A*, 190, 275

Lagrange, A.-M., Vidal-Madjar, A., Deleuil, M., Emerich, C., Beust, H., & Ferlet, R. 1995, *A&A*, 296, 499

Lagrange, A.-M., et al. 1996, *A&A*, 310, 547

Lagrange, A.-M., et al. 1998, *A&A*, 330, 1091

Lagrange, A.-M., Backman, D. E., & Artymowicz, P. 2000, in *Protostars and Planets IV*, ed. V. Mannings, A. P. Boss, & S. S. Russell (Tucson: Univ. Arizona Press), 639

Lecavelier des Etangs, A., et al. 2001, *Nature*, 412, 706

Liseau, R. 2003, in *Towards Other Earths: DARWIN/TPF and the Search for Extrasolar Terrestrial Planets*, ed. M. Fridlund, T. Henning, & H. Lacoste (Noordwijk: ESA Publ. Division), 135

Martin, W. C., Fuhr, J. R., Kelleher, D. E., Musgrove, A., Sugar, J., Wiese, W. L., Mohr, P. J., & Olsen, K. 1999, NIST Atomic Spectra Database, (Gaithersburg, MD: NIST), version 2.0, <http://physics.nist.gov/asd2>

Mendis, D. A., & Rosenberg, M. 1994, *ARA&A*, 32, 419

Northrop, T. G., & Birmingham, T. J. 1990, *Planet. Space Sci.*, 38, 319

Northrop, T. G. & Birmingham, T. J. 1996, *J. Geophys. Res.*, 101, 793

Olofsson, G., Liseau, R., & Brandeker, A. 2001, *ApJ*, 563, L80

Rafikov, R. R. 2004, *AJ*, 128, 1348

Roberge, A., Weinberger, A. J., Feldman, P.D., Deleuil, M., & Bouret, J.-C. 2005, poster #8036 at Protostars and Planets V, Hawaii, USA

Royer, F., Gerbaldi, M., Faraggiana R., Gómez, A. E. 2002, *A&A*, 381, 105

Shu, F. H., Adams, F. C., & Lizano, S. 1987, *ARA&A*, 25, 23

Smith, B. A., & Terrile, R. J. 1984, *Sci*, 226, 1421

Spitzer, L. 1941, *ApJ*, 93, 369

Spitzer, L. 1956, *Physics of Fully Ionized Gases* (New York: Interscience)

Spitzer, L. 1978, *Physical Processes in the Interstellar Medium* (New York: Wiley)

Thébault, P., Augereau, J. C., & Beust, H. 2003, *A&A*, 408, 775

Thébault, P., & Augereau, J. C. 2005, *A&A*, 437, 141

Thi, W. F., et al. 2001, *Nature*, 409, 60

Weinberger, A. J., Becklin, E. E., Zuckerman, B. 2003, *ApJ*, 584, 33

Weingartner, J. C., & Draine, B. T. 2001, *ApJ*, 134, 263

Zuckerman, B., Song, I., Bessel, M. S., & Webb, R. A. 2001, *ApJ*, 562, L87